Simulation of long-term thermo-mechanical response of clay using an advanced constitutive model

As Published: https://doi.org/10.1007/s11440-018-0726-6

Publisher: Springer Berlin Heidelberg

Persistent URL: https://hdl.handle.net/1721.1/131384

Version: Author's final manuscript: final author's manuscript post peer review, without publisher's formatting or copy editing

Simulation of Long-Term Thermo-Mechanical Response of Clay Using an Advanced Constitutive Model

by

Despina M. Zymnis[1], Andrew J. Whittle[2] and Xiaohui Cheng[3]

ABSTRACT

There is extensive data to show that heating and cooling produces irrecoverable deformations in clays under fully drained conditions. The effects are most pronounced for normally and lightly overconsolidated clays that undergo significant compression. Most constitutive models have key limitations for predicting the thermo-mechanical response of clays through long-term (seasonal) cycles of heating and cooling. The Tsinghua ThermoSoil model (TTS; Zhang & Cheng, 2017) presents a novel theoretical framework for simulating the coupled thermo-mechanical response of clays. The model uses a double entropy approach to capture effects of energy dissipation at the microscopic particulate contact level on continuum behavior. This paper proposes a simple procedure for calibrating input parameters and illustrates this process using recent lab data for Geneva clay (Di Donna and Laloui, 2015). We then investigate capabilities of the TTS model in simulating familiar aspects of thermal consolidation of clays as well as the long-term, progressive accumulation of strains associated with seasonal heating and cooling processes for shallow geothermal systems installed in clays.

The model predicts the existence of a long-term steady state condition where there is no further accumulation of strain. This state depends on the consolidation stress and stress history but is independent of the imposed range of temperature, T_{cyc}. However, the value of T_{cyc} does affect the rate of accumulation of strain with thermal cycles. Simulations for normally consolidated Geneva clay find steady state strain conditions ranged from 2.0 to 3.7% accumulating within N = 10 - 50 thermal cycles.

[1] Former Ph.D. student, Department of Civil & Environmental Engineering, MIT, Cambridge, MA 02139
[2] Edmund K. Turner Professor of Civil & Environmental Engineering, MIT, Cambridge, MA 02139
[3] Associate Professor of Civil Engineering, Tsinghua University, Beijing, 100084, China

1. Introduction

The thermo-mechanical response of clays has been studied in the context of applications including nuclear waste disposal (e.g., Gens, 2003; Gens & Olivella, 2001b, 2005; Gens et al., 2009a&b; Gens, 2010), energy foundations (e.g., Laloui et al., 2003, 2006) and seasonal ground heat storage (e.g., Zymnis, 2016). Laboratory measurements show that temperature changes can significantly alter the properties of clays and induce permanent deformations (Baldi et al., 1991; Campanella and Mitchell, 1968; Hueckel and Baldi, 1990; Abuel-Naga et al., 2006; Cekerevak and Laloui, 2004). These effects become more pronounced when cyclic heating and cooling is imposed (e.g., due to the continuous operation of ground source heat pumps) and can generate significant long-term settlements (Campanella and Mitchell, 1968; Hueckel et al., 1998; Di Donna and Laloui, 2015). Zymnis and Whittle (2014) have shown cyclic thermal loading induced by borehole heat exchangers can lead to thermal volumetric strains and hence, the study of cyclic thermal loading is crucial when designing shallow geothermal installations.

Existing thermo-elastic constitutive models (e.g., Booker and Savvidou, 1985; Smith and Booker, 1989) cannot describe irreversible thermal strains. More advanced thermo-elastoplastic constitutive models are macroscopic, usually based on an extension of the Cam-Clay model to account for temperature (e.g., Hueckel and Borsetto, 1990; Hueckel and Baldi, 1990; Laloui and Francois, 2009) and can describe thermal response reasonable well. However, their validity beyond experimental results is questionable since the physical processes at the microscale are not accounted for. Furthermore, most constitutive models have key limitations for predicting the thermo-mechanical response of clays through long-term (seasonal) cycles of heating and cooling. For example in the model proposed by Hueckel and Borsetto (1990), all of the irreversible strain takes place during the first heating and cooling cycle and the model is incapable of describing accumulation of irreversible thermal strain thereafter. Di Donna and Laloui (2015) extend the ACMEG-T model (Laloui and Francois, 2009) to account for irreversible strain accumulation, using “the cyclic plastic radius” that makes the model much more complex, without basing the soil response on physical processes. The Tsinghua Thermosoil model (TTS; Zhang and Cheng, 2017) associates the accumulation of volumetric strain during continuous cycles of heating and cooling with the exchange

between bound (i.e., adsorbed on clay particles) and free water. The underlying basis for TTS is supported by recent molecular simulations presented by Brochard et al. (2017), who relate macroscopic thermo-mechanical response of clay to water adsorption at the nanoscale. The TTS model, is the first constitutive model capable of describing macroscopic thermo-mechanical clay while accounting for physical processes at the microscale.

The current paper has implemented the TTS model to study 1-D settlements due to seasonal cycles of heating and cooling. The paper begins with a review of the main concepts of the TTS model formulation and clarifies the simplifications assumed for the current application. One key aspect of the TTS model relates to the thermal effects on the conversion of 'bound water' (i.e., water adsorbed onto the surface of clay particles, e.g., Lambe, 1960; Paaswell, 1967; Morin and Silva, 1984; Delage et al., 2000) to free water. The paper proposes simple and effective calibration techniques for TTS parameters related to thermo-mechanical effects and illustrates this methodology using recent lab data for Geneva Clay (Di Donna and Laloui, 2015). The paper concludes with an in-depth evaluation of the TTS model, with an emphasis on the simulation of clay response to long-term cyclic heating and cooling.

2. Tsinghua Thermosoil (TTS) Model Formulation

The TTS model is based on non-equilibrium thermodynamic theory (Groot and Mazur, 1962) in order to provide a more fundamental physical basis for characterizing the complex (transient and steady state) behavior of geomaterials, based on the framework of Granular Solid Hydrodynamics (GSH; Jiang and Liu, 2007). The current application considers the thermo-mechanical behavior of clays and can be contrasted with prior models based on classical elasto-thermoplasticity (e.g., Hueckel and Borsetto, 1990; Cui et al., 2000; Laloui and Francois, 2009). The TTS model does not use a yield function, flow rules or other constraints of classical plasticity, but is able to describe many key empirical observations of clay behavior, including virgin consolidation of normally consolidated clay and hysteretic stress-strain response in unloading and reloading. The current implementation of the TTS model makes the following assumptions:

1. Soil is fully saturated (for isothermal conditions, deformation and shear strength are controlled by effective stresses) and is composed of a mixture of solid and liquid phases (Figure 1).
2. All three phases are continuous in space and have the same temperature.
3. There is no phase change in water for the temperature range considered (i.e., no solidification or vaporization).

The liquid phase is divided into free water, which fully fills the macroscopic pores and whose migration is described by Darcy's Law; and bound water, which is fully adsorbed by the soil particles and fills the microscopic pore space (for sands, the specific surface area is small, SSA ~ 0.03 m^2/g while for clay particles SSA can range from 10-270 m^2/g, with the highest values for smectites). The total porosity, φ, and dry density of solid particles, ρ_d, are then given by:

$$\phi = \phi_{fw} + \phi_{bw} \tag{1}$$

$$\rho_d = G_s \rho_{fw} (1 - \phi) \tag{2}$$

where G_s is the specific gravity of soil, and ρ_{fw} is the density of free water.

The thermal response of clays is often linked to physicochemical clay-water interactions, based on the mass transfer of bound water from a solid state to a fluid state (Hueckel, 1992). At elevated temperatures, part of the bound water is converted to free water, which in turn produces irreversible reorganization of the clay particles and thermal irreversible strains. Zhang and Cheng (2017) have proposed an exponential decay function relating changes in bound water content, w_{bw}, to temperature, T:

$$w_{bw} = w_{bw,20} \exp\left[-\alpha_{bf} (T - 20)\right], \quad T \left[^{o}C\right] \tag{3a}$$

where $w_{bw,20}$ is the bound water content at 20°C and α_{bf} [1/°C] is a characteristic material property:

$$\alpha_{bf} = -\frac{1}{w_{bw}} \frac{\partial w_{bw}}{\partial T} \tag{3b}$$

Zymnis et al. (2019a) performed a series of experiments that study this process through measurements of temperature-dependence in the specific gravity of the solid particles. Three clays of widely differing mineralogy were tested: 1) Kaolinite, with a specific surface area, SSA = 14 m^2/g; 2) illite-rich, Boston Blue Clay (BBC Series IV)

with SSA = 49 m^2/g; and 3) smectite-rich, Eugene Island (EI-GOM) clay sourced from the Gulf of Mexico, with SSA = 267 m^2/g. The laboratory experiments confirm that the specific gravity of clays decreases with temperature consistent with the conversion of bound water to free water. Figure 2 presents the estimated change of bound water content with temperature for all three clays, by assuming a mass density of bound water $\rho_{bw}(T) = 1.07\rho_{fw}(T)$, based on pycnometer measurements reported in the literature (De Wit and Arens 1950; Mackenzie, 1958; Mooney et al., 1952; Norrish, 1954; Anderson and Low, 1958) and assuming that the adsorbed water layer adjacent to clay minerals has a thickness of about three water molecules as reported by several authors (e.g., Fripiat et al., 1984; Sposito, 1984; Sposito and Prost, 1982; Mitchell, 1993; Suter et al, 2007). The bound water content at 20°C estimated for EI-GOM clay is $w_{bw,20}$ = 24% which is considerably higher than that for BBC ($w_{bw,20}$ = 5%) and Kaolinite ($w_{bw,20}$ = 1%). For a temperature increase of 20°C, the bound water content of EI-GOM clay decreases by ~4%, while reductions for BBC and Kaolinite are ~1.2% and ~0.3%, respectively.

In the current formulation we use the following evolution of bound water porosity:

$$\dot{\phi}_{bw} = -\phi_{bw}\left(\alpha_{bf} - \frac{\beta_w}{1-\beta_w \Delta T}\right)\dot{T} \qquad (4)$$

where β_w is the thermal expansion coefficient of water ($\beta_{w,vol}$ = 3.4 x 10^{-4}/°C). We assume that bound water porosity is not affected by changes in total volumetric strain (i.e., deformations of the soil skeleton only change the free water porosity).

The TTS model accounts for interactions between the continuum (macro-level) and micro-level (i.e., particle or granular level) behavior through a double-entropy formulation. The total entropy is used to describe macroscopic phenomena (irrecoverable deformations), while the granular entropy represents microscopic phenomena (sliding, rolling and collision of particles, which results to a change in their kinetic energy and elastic potential energy; Figure 3). It is assumed that once external loading is applied, there is a simultaneous increase in both total and granular entropies and granular entropy is subsequently converted to total entropy at a rate, $\dot{I}_g$[J/m^3s]. The energy generation at the microscopic scale is the source of plastic deformation for granular solids and is attenuated by heat generation at the macro-level. Jiang and Liu (2009) proposed that

energy generation at the microscopic level is similar to molecular motion and can be described through a granular entropy density and its conjugate variable, granular temperature, T_g [s^{-2}] (T_g is not the actual temperature, T). The evolution of granular temperature is given by:

$$\dot{T}_g = \frac{1}{\rho_d}\left[m_2 m_4 \left(\dot{\varepsilon}_s\right)^2 + m_2 m_3 m_4 \left(\dot{\varepsilon}_v\right)^2 + \frac{m_5 \sigma'_{oct} \alpha_{bf} \phi_{bw} \dot{T}^2}{\left(1-\phi\right)} - m_4 T_g \right] \qquad (5)$$

where $\varepsilon_v = \varepsilon_{kk}$ is the volumetric strain and $\varepsilon_s = \sqrt{e_{ij} e_{ij}}, \left(e_{ij} = \varepsilon_{ij} - \varepsilon_{kk}\delta_{ij}/3\right)$ is the second invariant of the deviatoric strain rate tensor, σ'_{oct} is the mean effective stress and m_2, m_3, m_4, m_5 are input constants (migration coefficients) for the TTS model.

External loading, either as a strain rate, $\dot{\varepsilon}_{ij}$ or temperature rate, $\dot{T}$, increases the granular temperature, T_g (first three terms of eqn. 5). The current simplified version of the TTS model assumes m_3 = 1 and represents the case where volumetric and shear components contribute equally to the evolution of granular temperature. The third term of the right-hand side of eqn. 5 reflects the irrecoverable particulate level movement induced by the conversion of bound to free water to simulate the irreversible volumetric deformation caused by changes in temperature (cf., eqns. 3a and 3b).

It is assumed that m_5 = 0 for $\dot{T} \le 0$, since cooling does not produce irreversible thermal strain, as confirmed in experimental tests (e.g., Baldi et al., 1991). The fourth term (i.e., $m_4 T_g$) is a damping component while m_4 controls the time lag required for T_g to reach steady state conditions.

The total strain rate $\dot{\varepsilon}_{ij}$ is the sum of elastic strain rate, $\dot{\varepsilon}^e_{ij}$, and 'irrecoverable' strain rate, $\dot{\varepsilon}^D_{ij}$, as shown below:

$$\dot{\varepsilon}^e_{ij} = \dot{\varepsilon}_{ij} - \dot{\varepsilon}^D_{ij} \qquad (6a)$$

Figure 4a illustrates the prediction of cyclic strain accumulation due to mechanical loading and unloading (cf., eqn. 6c). The shear strain rate is linked to the current granular temperature and elastic shear strain. In order to avoid overestimation of strain accumulation (large ratcheting strains, Figure 4a), Zhang and Cheng (2013) introduced a 'hysteretic' strain, ε^h_{ij}, as an additional state variable in the TTS model

formulation, such that each cycle of loading produces smaller net irrecoverable strain (Figure 4b). The evolution of irrecoverable strain rate, $\dot{\varepsilon}_{ij}^{D}$, is expressed as a function of granular temperature T_g and the elastic and hysteretic strains:

$$\dot{\varepsilon}_v^D = 3m_1\left(T_g\right)^a\left(\varepsilon_v^e - \varepsilon_v^h\right) \tag{6b}$$

$$\dot{\varepsilon}_s^D = \left(T_g\right)^a\left(\varepsilon_s^e - \varepsilon_s^h\right) \tag{6c}$$

where the migration coefficient $m_1 = m_{1,0}\left[1 + L_T\left(T - T_0\right)\right]$ (we are assuming $m_{1,0} = 1$), T_0 is a reference temperature, L_T [1/°C] is an input constant that describes the dependence of parameter m_1 on temperature and a is a parameter that controls rate dependence (Appendix A shows that $a = 0.5$ produces rate independent virgin consolidation states).

The evolution of the volumetric and deviatoric components of hysteretic strain assumed in the current implementation are:

$$\dot{\varepsilon}_v^h = \dot{\varepsilon}_v^D - \frac{\frac{1}{3}\dot{\varepsilon}_v^D\varepsilon_v^h + \dot{\varepsilon}_s^D\varepsilon_s^h}{h^{0.5}\left[\frac{1}{3}\left(\varepsilon_v^h\right)^2 + \left(\varepsilon_s^h\right)^2\right]^{0.75}}\varepsilon_v^h \tag{7a}$$

$$\dot{\varepsilon}_s^h = \dot{\varepsilon}_s^D - \frac{\frac{1}{3}\dot{\varepsilon}_v^D\varepsilon_v^h + \dot{\varepsilon}_s^D\cdot\varepsilon_s^h}{h^{0.5}\left[\frac{1}{3}\left(\varepsilon_v^h\right)^2 + \left(\varepsilon_s^h\right)^2\right]^{0.75}}\varepsilon_s^h \tag{7b}$$

where parameter h is an input constant.

Since the evolution of irrecoverable strain rate depends on granular temperature, T_g, it becomes apparent that the application of external loading will increase the granular temperature and will also produce irrecoverable strain (cf., eqns. 5, 6b and 6c). Figure 5 illustrates TTS simulations of the time-varying response of mean effective stress to a step change in applied volumetric strain (for Geneva clay) for an element undergoing hydrostatic compression. Higher values of m_4 produce rapid convergence to steady state conditions (for m_4 = 1000 kg/m^{3}s, the stress reaches its constant value in 5s while for m_4 = 100 kg/m^{3}s, the stress equilibrates in 30s). The current application focuses on steady state conditions and hence, we assume a large value of $m_4 = 6\times10^4$ kg/m^{3}s.

The TTS model assumes that reversible energy processes result in locked-in elasticity in the system that can be expressed by an elastic potential energy function. The effective stress state is expressed as the derivative of the elastic potential energy density function, ω_e:

$$\sigma'_{ij} = \frac{\partial \omega_e}{\partial \varepsilon^e_{ij}} \tag{8}$$

This definition is common to all 'hyperelastic' models of soil behavior (e.g., Houlsby and Puzrin, 2007). Zhang and Cheng (2017) propose an expression for ω_e that limits the range of possible stress states (reflecting limits on cohesive and frictional shear strength components) and includes thermal elastic strains of the solid minerals:

$$\omega_e = \frac{2}{5} B \left(\varepsilon^e_v + c\right)^{1.5} \left(\varepsilon^e_v\right)^2 + B\xi \left(\varepsilon^e_s\right)^2 \left(\varepsilon^e_v + c'\right)^{1.5} + \int 3K_e \beta_s \left(T - T_0\right) d\varepsilon^e_v \tag{9}$$

where $B = B_0 \exp(B_1 \rho_d)$, B_0, B_1, c, ξ, c' are input constants, β_s is the linear thermal expansion coefficient for the solid skeleton and K_e is the secant elastic bulk modulus of the solid skeleton:

$$K_e = 0.6B\left(\varepsilon^e_v + c\right)^{0.5} \varepsilon^e_v + 0.8B\left(\varepsilon^e_v + c\right)^{1.5} + 1.5B\xi\left(\varepsilon^e_v + c'\right)^{0.5} \frac{\left(\varepsilon^e_s\right)^2}{\varepsilon^e_v} \tag{10}$$

By combining eqns. 8 and 9, the mean effective stress and deviatoric stress can be expressed by:

$$\begin{aligned} p' &= K_e\left(\varepsilon^e_v + 3\beta_s \Delta T\right) \\ q &= \sqrt{6} B \xi \varepsilon^e_s \left(\varepsilon^e_v + c'\right)^{1.5} \end{aligned} \tag{11}$$

It is subsequently shown that B_0 and B_1 can be related to the location and slope of the virgin consolidation line, respectively; c is linked to cohesion of soils ($c = 0$ for sands; here we assume a nominal value, c = 0.01 for reconstituted clays); ξ is related to the size of the state boundary surface (i.e., limit on possible effective stress states that is linked to maximum allowable ratios of shear to normal stress) and affects the peak internal friction and the in-situ coefficient of earth pressure at rest K_0 ($=\sigma'_h/\sigma'_v$) and c' controls the critical state friction angle.

Zhang and Cheng (2017) derive the state boundary surface, also referred to as the Ultimate Stress State Surface (USSS) from the singularity condition of the Hessian

matrix, $\det|\omega_e| = 0$. Panagiotidou (2017) presents an in-depth study of the shear response of the TTS model in relation to critical state soil mechanics and shows that the slope, *M*, of the Critical State Line (CSL) is simulated by the TTS model and can be derived as (see Appendix B):

$$M = \frac{q_f}{p'_f} = \frac{\sqrt{6}c'}{1.5\left(h + \frac{1}{\sqrt{m_2}}\right)} \tag{12}$$

Table 1 summarizes the state variables used in the TTS model, which comprise the bound and free water porosity, φ_{bw} and φ_{fw}, the temperature, *T*, the granular temperature, T_g, the total strain, ε, elastic strain, ε^e, and hysteretic strain, ε^h, (with subscripts *v* and *s* corresponding to volumetric and deviatoric invariants, respectively). Table 2 shows the material input parameters, while Section 4 describes their calibration in detail.

3. Cyclic Thermal Tests on Geneva Clay

Di Donna and Laloui (2015) carried out a series of drained thermal cyclic tests on samples of medium plasticity silty clay from Geneva, Switzerland (I_p = 11 - 19%, w = 22 - 28%). As there are very few cyclic thermal tests reported in the literature (notable exceptions include data presented by Campanella and Mitchell, 1968; Hueckel et al., 1998) these tests are very useful in evaluating TTS model capabilities for representing the accumulation of long-term thermal movements induced in clay. The soil samples were collected from a site near Geneva as part of a project involving the construction of a new building and the installation of a large array of borehole heat exchangers for space heating and cooling. Table 3 shows the in-situ state of stress (normally consolidated clay) and index properties for samples S3 and S4b, which are considered here. The samples are saturated and have a fines fraction (d < 2μm) between 38 - 45%.

Two sets of experiments were undertaken: i) 1-D oedometric compression tests at different constant temperatures; and ii) thermal cycles under constant vertical effective stress. Details of the laboratory procedure are provided by Di Donna and Laloui (2015) and are summarized in Table 4. Figure 6 presents the oedometric test results (in the

conventional void ratio e – logσ_v' space, where e = $\varphi/(1-\varphi)$) on sample S3 at temperature T = 20°C, 40°C and 60°C for the entire duration of the test. Sample S3 was initially equilibrated at the selected temperature at a nominal vertical stress of 1kPa (weight of top cap). Once the temperature and deformation were stable, incremental load sequences were performed, with loading steps up to 1000kPa and unloading to 60kPa. It is observed that all consolidation curves are parallel and so the compressibility index (C_c = -de/d$\log_{10}\sigma'_v$) of Geneva clay at a given stress is unaffected by temperature, thus confirming trends reported previously in the literature (e.g., Hueckel et al., 1998). Figure 6a shows that the main effect of higher temperature is to increase density (reduce void ratio) at a given effective consolidation stress (i.e. the void ratio is lower at 40°C and 60°C than at 20°C at a given effective consolidation stress). However, in contrast to prior results in the literature (e.g., Leroueil and Marques, 1996) the data do not show a clear monotonic trend with temperature.

Di Donna and Laloui (2015) studied the effect of combined thermal and mechanical loading of Geneva Clay sample S4b. Figure 6b shows that the material was first consolidated to 125 kPa (from point 1 to point 2) at ambient temperature T = 20°C, then subjected to four thermal cycles (with a temperature range between 5°C and 60°C, from point 2 to point 3) and finally loaded up to 2000 kPa (from point 3 to point 5) with an unloading phase, all at temperature T = 20°C. The cycles of heating and cooling generated an apparent overconsolidation of the specimen as subsequent loading (point 3 to point 5) involved a stiff response with yield at point 4, similar to prior results (e.g., Cekerevac and Laloui, 2004). This 'thermal hardening' effect is similar to drained creep (secondary compression) as reported by Leroueil and Marques (1996).

Figure 7 presents the results of the cyclic thermal tests undertaken on S3 samples (at OCR = 1 and 16). The NC samples were initially consolidated to the in-situ vertical effective stress ($\sigma'_{v0} \sim \sigma'_p$) at ambient temperature, T = 20 °C, and then thermal cycles were performed in the range between 5°C and 60°C. Vertical displacements were recorded throughout the experiments and the heating phases were applied in steps of 10°C, imposing a heating rate of 2°C per hour in order to ensure drained conditions and thus provide enough time for excess pore water pressure dissipation. The cooling phases were applied in steps of 20 °C and with a cooling rate of 5°C/h. Thermal cycling of the

OC specimen resulted in small dilative strains ($\varepsilon_v \approx -0.1\%$) similar to prior results (e.g., Baldi et al., 1991; Cekerevac and Laloui, 2004). Assuming that the measured deformation corresponds to the thermo-elastic expansion and compression of the solid skeleton, Di Donna and Laloui (2015) computed the volumetric thermal expansion coefficient of the solid skeleton equal to $\beta_{s,vol} = 1.8\times10^{-5}°C^{-1}$. On the other hand, cyclic heating and cooling of NC clay specimens results in larger irreversible contractive strains (with accumulated volume strain, $\Delta\varepsilon_v \approx 0.6 – 0.9\%$).

4. TTS Model Calibration for Geneva Clay

The following paragraphs present our proposed method for calibrating the TTS model and illustrate this process for intact specimens of Geneva clay. Initial values of the state variables can be derived by consolidating from a reference slurry state ($\sigma'_{v0} = 0$ kPa) with void ratio e = 2.0 (porosity $\varphi = 0.5$ and bound water porosity $\varphi_{bw} = 1\%$, based on results for Kaolinite; c.f., Figure 2) and assuming that the other state variables shown in Table 1 are initially zero at ambient temperature, T_0 = 20°C. The model is driven by specified rates of strain, $\dot{\varepsilon}$, and temperature, $\dot{T}$ (eqns 5, 6a and 6b).

It should be noted that using the Specimen Quality Designation (SQD) method recommended by Ladd and DeGroot (2003), the samples S3 and S4b are highly disturbed (Figures 6a and 6b show that the vertical strains measured at 20°C at σ'_{v0} are 6.3% and 8.7% for S3 and S4b, respectively). These results imply that the compression index, C_c, will be systematically underestimated. Calibration of the VCL was based on the sample S4b measurements.

Mechanical Components

The main input constants that control the 1-D compression response of clays are B_0, B_1, m_2, h, and ξ (Table 2). The clay was loaded from an initially slurry condition to a void ratio e = 0.63, unloaded to void ratio e = 0.7 and reloaded to e = 0.57 (the void ratios correspond to those reached by sample S4b during the lab experiments). Figure 8 presents results for normalized vertical stresses (σ'_v/σ'_{ref}, where σ'_{ref} is the vertical stress calculated by the TTS model at void ratio e = 0.63, where unloading begins). The slope of the VCL increases as B_1 decreases and B_1 = 0.0162 m^3/kg provides a good fit to the

measured data. Parameter *h* controls the slope of the unload curve as shown in Figure 9a, with larger unloading slopes occurring for larger *h* (eqn. 7). Figure 9b shows that the reloading response depends on parameter m_2, with larger m_2 affecting the reloading branch of the test.

For a friction angle φ = 24°, determined by triaxial tests on Geneva clay (Di Donna, 2014) the slope, *M*, of the critical state line:

$$M = \frac{6\sin\phi}{3-\sin\phi} = 0.94 \tag{13}$$

from which *c'* can be obtained using eqn. 12:

$$c' = \frac{1.5\left(h+\frac{1}{\sqrt{m_2}}\right)}{\sqrt{6}} M = \frac{1.5\left(0.05+\frac{1}{\sqrt{150}}\right)}{\sqrt{6}} 0.94 = 0.0758 \tag{14}$$

For normally consolidated clay, K_{0NC} increases with decreasing ξ (i.e., horizontal stresses are larger for smaller ξ while vertical stresses remain unchanged). Assuming K_{0NC} = 0.6 (using eqn. 15 suggested by Jâky, 1944) for Geneva Clay with friction angle of 24°, ξ = 0.1 (Figure 10).

$$K_{0NC} = 1-\sin\phi \tag{15}$$

The TTS model predicts K_{0OC} decreasing with OCR contrary to established soil behavior. This represents a notable limitation of the model that should be addressed in future research but has little effect on the model capabilities in describing accumulation of 1-D settlements under cyclic thermal loading (Zymnis, 2016).

The final part of the mechanical calibration involves setting the reference void ratio for the VCL by calibrating parameter B_0 (eqns. 10 & 11). Figure 11 illustrates that the reference void ratio (i.e., *e* at a selected σ'_v) increases with B_0 and shows good agreement with data for Geneva Clay for $B_0 = 3.8\times10^{-4}$ Pa. It should be noted that all of the input constants affect the location of the VCL and hence, parameter B_0 must be chosen last in the calibration process.

Figure 12 presents the resulting TTS fit for Geneva Clay sample S4b using the calibrated parameters shown in Table 2. The loading steps followed are:

1 – 2: 1-D Consolidation from an initially slurry condition up to σ_v' = 230kPa

2 – 3: 1-D Unloading to σ_v' = 1kPa

3 – 4: Reloading to σ_v' = 1MPa

4 – 5: Unloading to σ_v' = 60kPa

5 – 6: Reloading to σ_v' = 3MPa

Figures 12c and 12d present the evolution of the strain state variables $\left(\varepsilon_v^e, \varepsilon_v^h, \varepsilon_s^e, \varepsilon_s^h\right)$ of the TTS model during these steps. All internal strains start from zero in the slurry condition (point 1) and reach a constant value once the clay is consolidated along the VCL (σ_v' ~ 1kPa, Figure 12a). This condition occurs as the TTS model assumes there is a fixed amount of locked-in elasticity in the normally consolidated stress states. During unloading (step 2 - 3) the volumetric (elastic and hysteretic) strains and elastic deviatoric strains decrease (Figures 12c and 12d) and increase again during reloading, while the hysteretic deviatoric strains (ε_s^h; Figure 12d) have the opposite response. The primary state variable that changes when compressing a NC clay on the VCL is the void ratio, e (and corresponding dry density, ρ_d). Figures 12b and 13 show that the TTS model describes closely the 1-D compression behavior of natural Geneva Clay (samples S3 and S4b) measured by Di Donna and Laloui (2015).

Thermal Components

The input constants that control the thermal behavior of the TTS model are α_{bf}, L_T and m_5. Based on index properties it is concluded that Geneva Clay will have similar α_{bf} parameter to BBC and Kaolinite and thus α_{bf} = 0.0237°C^{-1} (cf., Figure 2).

The parameter L_T affects the temperature dependence of the VCL (eqn. 6b), with larger L_T resulting in a more pronounced effect of temperature. Figure 13 shows that the best overall agreement is achieved for L_T = 0.020°C, which is used in all subsequent calculations. The measurements at T = 40°C have not been used for calibration since as already discussed (cf., Figure 6a) they do not show a monotonic response with temperature, in contrast to prior results in the literature and hence have been omitted from the figure.

Figures 14b-d illustrate the effect of selected values of m_5 (eqns. 5 and 6b) on predictions of thermal volumetric strains for cyclic tests at OCR = 1.0 and 16.0 (sample

S3). As m_5 increases, the accumulation of compressive strains for NC clay and dilative strains for OC clay both increase. For Geneva Clay, using $m_5 = 0.1 s^3 m^{-2\,o} C^{-1}$ accurately described the thermal volumetric strain induced during the first heating cooling cycle for NC clay and results in 0.4% larger thermal strain accumulation after 4 cycles of heating-cooling compared to the lab measurements shown in Figure 14b. These effects are accentuated at higher values of m_5. For the case of the OC clay, the TTS model generally overestimates the dilative strains (accumulated in 4 cycles) by 0.6%.

It can be readily seen that the TTS model calibration proposed herein is straightforward and the parameters can be obtained from independent tests, typically performed in the lab.

5. Evaluation of Model Predictions for Long-Term Response to Cycles of Heating and Cooling

Figure 15 shows TTS simulations for a single cycle of heating and cooling at different initial OCRs, under constant vertical stress. The results show that the TTS model provides a reasonable estimate of thermal volumetric strains at different stress levels with a transition to dilative response in the range OCR = 2.0 – 4.0. Moreover, the TTS model predicts that the thermal volumetric strains are always irreversible even for OC clays, something that has been reported in some thermal tests in the literature, although prior models generally suggest elastic response for OC clays (e.g., Hueckel and Borsetto, 1990; Laloui and Francois, 2009). Figure 15b shows the porosity of bound water against temperature. As expected, the conversion of bound water to free water is a reversible process that is independent of OCR (cf. eqn. 4b). An increase in temperature from 20°C to 60°C causes a decrease in bound water porosity $\Delta\varphi_{bw}$ = -0.6% (φ_{bw} = 1% at 20°C and φ_{bw} = 0.4% at 60°C), while at 5°C, φ_{bw} = 1.4%. Figure 15d presents the evolution of elastic and hysteretic volumetric strains during loading to σ_v' = 125kPa and unloading to vertical stress σ_v' corresponding to the different OCRs. At σ_v' = 60kPa, where $\varepsilon_v^e = \varepsilon_v^h$ the resulting thermal volumetric strains computed by the TTS model are nearly zero as shown by the OCR = 2 line (Figure 15c). For vertical stress σ_v' > 60kPa (i.e. lower OCR) the resulting thermal volumetric strains are contractive while for σ_v' <

60kPa (i.e. higher OCR) the resulting thermal volumetric strains are dilative (Figures 15c and d).

Figure 16 illustrates the long-term cyclic strain accumulation simulated by TTS for initial OCR's = 1.0 – 8.0 for the temperature range used in lab tests on Geneva Clay (T = 5°C - 60°C, T_{ave} = 32.5°C). Continuous heating and cooling of NC clay (at vertical stress σ_v'=125kPa) results in long-term accumulation of contractive strain, ε_v = 2.0%; while similar thermal cycles produce ε_v = 3.66% at σ_v' =1MPa. Continuous heating and cooling of highly overconsolidated clay (OCR = 8) results in long-term accumulation of dilative volumetric strain (ε_v = 1.24%), while clays of intermediate OCR produce smaller accumulated strain (Figure 16c). The TTS model provides a good fit to the laboratory measurements on NC Geneva Clay (Test #7 on S3 sample, Figure 16c). The accumulation of volumetric strain reaches a limit when $\varepsilon_v^e = \varepsilon_v^h$ as shown in Figure 16d. In fact, long-term cyclic heating and cooling induces a steady state condition shown in Figure 16a that depends on the mechanical calibration of the TTS model (controlled by parameters h and m_2).

Figure 17 shows the strain accumulation for cycles of heating and cooling with T_{cyc} = ±5°C to ±20°C (and T_{ave} = 20°C). The TTS model predicts that heating and cooling of normally consolidated Geneva Clay ultimately trends to the same maximum volumetric strain (ε_v = 2.0%) independent of the imposed temperature range, while rates of strain accumulation are directly linked to the imposed cyclic range, T_{cyc}. For example, with T_{cyc} = ±20°C, the maximum strain accumulates within 40 cycles, while for T_{cyc} = ±5°C, the maximum strain develops in 150 cycles. Figures 16 and 17 demonstrate the capabilities of the TTS model to describe volumetric strain accumulation due to continuous heating and cooling. Although, there are currently no laboratory data to validate these results and the existence of a steady state is still a hypothesis, the model offers a useful framework to assess the long-term ground settlements due to seasonal heating and cooling of clays.

6. Summary and Conclusions

The Tsinghua ThermoSoil model (TTS; Zhang & Cheng, 2017) presents a novel theoretical framework for simulating the coupled thermo-mechanical properties of clays.

To our knowledge, it is the only model that can describe volumetric accumulation due to cyclic heating and cooling of clay, while accounting for physical processes. The model uses a double entropy approach (following the Granular Solid Hydrodynamics framework of Jiang & Liu, 2009) to capture effects of energy dissipation at the microscopic particulate contact level on continuum behavior and is capable of describing strain rate and thermal dependence in clay properties. The conversion of bound to free water represents a key concept that controls irreversible thermo-mechanical strains in the TTS model. This paper proposes simple and effective calibration techniques of the TTS model, and demonstrates them using recently published cyclic thermal tests on Geneva Clay (Di Donna and Laloui, 2015). The paper illustrates the TTS model capabilities in simulating familiar aspects of thermal consolidation of clays as well as the long-term, progressive accumulation of strains associated with seasonal heating and cooling processes for shallow geothermal systems installed in clays. Although there is limited experimental data for the behavior of clay subjected to a large number of thermal cycles, the model provides a useful framework for evaluating the thermo-mechanical response of clay and suggests the existence of a long-term steady state condition. Further laboratory studies of thermo-mechanical properties of different types of clay are needed to evaluate these TTS modeling capabilities.

Acknowledgements

The Authors are grateful for the support provided by the Low Carbon Energy University Alliance (LCEUA), which enabled three way collaborations with colleagues at Tsinghua University and the University of Cambridge. The first Author (DMZ) also received a Robert A. Brown, Onassis Foundation, Exponent and Martin Foundation Fellowships for her Ph.D. studies.

APPENDIX A

The TTS model accounts for strain rate dependence through parameter *a* shown in eqns. 6b and 6c. Figure A1 presents hydrostatic compression of Geneva clay, as simulated by the TTS model, assuming different strain rates. Using a = 0.5 results in a unique response (cf., solid lines overlap in Figure A1), providing rate independence of the model. On the other hand using a = 0.3 (dashed lines) results in different VCLs for different strain rates. An increase in rate of strain results in a decrease in density (increased void ratio) at a given effective consolidation stress (i.e., the void ratio is higher at $\dot{\varepsilon}_v = 0.05/\min$ than at $\dot{\varepsilon}_v = 0.001/\min$ at a given effective consolidation stress). The effect of strain rate is similar to the effect of temperature (cf., Figure 6a) since they both affect the viscous deformation of soils, as reported previously in the literature (e.g., Leroueil and Marques, 1997).

Figure A.1: Effect of input constant, *a*, on rate dependence assumed in TTS model

APPENDIX B

Panagiotidou (2017) studied the TTS model behavior at Critical State assuming undrained triaxial shearing with axial strain $\dot{\varepsilon}_a$, under isothermal conditions (i.e., $\dot{T}=0$). The resulting total volumetric and deviatoric strain rates are $\dot{\varepsilon}_v=0$ and $\dot{\varepsilon}_s=\sqrt{2/3}\dot{\varepsilon}_a$ respectively. At Critical State the soil reaches steady state conditions with constant deformations without change in volume or stresses $\dot{\varepsilon}_{vf}=\Delta p'_f=\Delta q_f=0$ and so all internal state variables are constant (cf., Table 1). Therefore, since the change of elastic strain is zero, the plastic strain is equal to the total applied strain:

$$\dot{\varepsilon}_v^D=\dot{\varepsilon}_v=0 \tag{B.1a}$$

$$\dot{\varepsilon}_s^D=\dot{\varepsilon}_s=\sqrt{2/3}\dot{\varepsilon}_a \tag{B.1b}$$

From eqn. 5 under isothermal conditions and assuming that $\dot{T}_g=0$, the granular temperature at critical state becomes:

$$T_{gCS}=m_2\left(\dot{\varepsilon}_s\right)^2 \tag{B.2}$$

From eqn. 7b, given that $\dot{\varepsilon}_s^h=0$ and $\dot{\varepsilon}_v^D=0$:

$$\varepsilon_s^h=h \tag{B.3}$$

In order for $\dot{\varepsilon}_v^h=0$, it is deduced from eqn. 7a that:

$$\varepsilon_v^h=0 \tag{B.4}$$

For $\dot{\varepsilon}_v^D=0$ and using eqn. 6a:

$$\varepsilon_v^e=\varepsilon_v^h=0 \tag{B.5}$$

From eqn. 6b and assuming rate independence (i.e., a = 0.5):

$$\dot{\varepsilon}_s^D = \left(T_g\right)^{\alpha}\left(\varepsilon_s^e - \varepsilon_s^h\right) = \left[m_2\left(\dot{\varepsilon}_s^D\right)^2\right]^{\alpha}\left(\varepsilon_s^e - \varepsilon_s^h\right)$$
$$\because \varepsilon_s^e = h + \frac{1}{\sqrt{m_2}} \tag{B.6}$$

The evolution of the stress components at Critical State can then be calculated (cf., eqn. 11):

$$p'_f = 1.5B\xi\left(c'\right)^{0.5}\left(\varepsilon_s^e\right)^2 \tag{B.7a}$$

$$q_f = \sqrt{6}B\xi\left(c'\right)^{1.5}\varepsilon_s^e \tag{B.7b}$$

Therefore, the slope of the critical state line, *M*, is given by the ratio of the deviatoric to the mean effective stress:

$$M = \frac{q_f}{p'_f} = \frac{\sqrt{6}c'}{1.5\left(h + \frac{1}{\sqrt{m_2}}\right)} \tag{B.8}$$

References

Abuel-Naga, H.M., Bergado, D.T., Ramana, G.V., Grino, L., Rujivipat, P. & They, Y. (2006) "Experimental evaluation of engineering behavior of Bangkok clay under elevated temperature," *ASCE Journal of Geotechnical and Geoenvironmental Engineering*, 132(7), 902-910.

Anderson, D. M. and Low, P. F. (1958), "The density of water adsorbed by Li-, Na-, and K-bentonite," *Soil Sci. Soc. Amer. Proc*., v. 22, pp. 99-103.

Baldi, G., Hueckel, T., Peano, A. & Pellegrini, R. (1991). Developments in modeling of thermo-hydro-geomechanical behaviour of Boom clay and clay-based buffer materials, Report 13365/2 EN. Luxembourg: Publications of the European Communities.

Booker, J.R. & Savvidou, C. (1985), "Consolidation around a point heat source," *International Journal for Numerical and Analytical methods in Geomechanics*, 9, 173-184.

Brochard, L., Honório, T., Vandamme, M., Bornert, M. & Peigney, M. (2017) "Nanoscale origin of the thermomechanical behavior of clays," *Acta Geotechnica*, 12, 1261-1279.

Campanella, R.G., and Mitchell, J.K. (1968), "Influence of temperature variations on soil behavior," *ASCE Journal of the Soil Mechanics and Foundation Engineering Division*, 94(SM3), pp. 709–734.

Cekerevac, C. (2003), "Thermal effects on the mechanical behaviour of saturated clays: an experimental and constitutive study," *Ph.D. Thesis*, École Polytechnique Federale de Lausanne

Cekerevac, C. and Laloui, L. (2004), "Experimental study of thermal effects on the mechanical behaviour of a clay," *International Journal for Numerical and Analytical Methods in Geomechanics*, 28(3), 209-228, doi: 10.1002/Nag.332.

Cui, Y. J., Sultan, N. & Delage, P. (2000), "A thermomechanical model for saturated clays," *Canadian Geotechnical Journal* 37, No. 3, 607–620.

Delage, P., Sultan, N. and Cui Y. J. (2000), "On the thermal consolidation of Boom clay," *Canadian Geotechnical Journal* 37: 343–354.

De Wit, C. T. and Arens, P. L. (1950), "Moisture content and density of some clay minerals and some remarks on the hydration pattern of clay," *Trans. 4th Int. Cong. Soil Sci.*, v. 2, pp. 59-62.

Di Donna, A. (2014), "Thermo-mechanical aspects of energy piles," Ph.D. Thesis, École Polytechnique Federale de Lausanne.

Di Donna, A. and Laloui, L. (2015), "Response of soil subjected to thermal cyclic loading: Experimental and constitutive study," *Engineering Geology* 190, pp. 65-76.

Fripiat, J. J., Letellier, M., and Levitz, P. (1984), "Interaction of water with clay surfaces," *Philosophical Transactions of the Royal Society of London*, A311, pp. 287-299.

Gens, A. & Olivella, S. (2001b), "Numerical analysis of radioactive waste disposal," *In Environmental geomechanics* (ed. B. A. Schrefler), pp. 203–234. Wien: Springer.

Gens, A. (2003), "The role of geotechnical engineering for nuclear energy utilization," *Proc. 13th. Eur. Conf. Soil Mech. Geotech. Engng*, Prague 3, 25–67.

Gens, A. & Olivella, S. (2005), "Numerical modelling in nuclear waste storage engineering," *Proc. 11th IACMAG Int. Conf.*, Turin 4, 555–570.

Gens, A., Garitte, B., Olivella, S. and Vaunat, J. (2009a), "Applications of multiphysical geomechanics in underground nuclear waste storage," *Eur. J. Env. Civil Engng* 13, No. 7–8, 937–962.

Gens, A., Sanchez, M., Guimaraes, L. do N., Alonso, E. E., Lloret, A., Olivella, S., Villar, M. V. & Huertas, F. (2009b), "A full-scale in situ heating test for high-level nuclear waste disposal: observations, analysis and interpretation," *Géotechnique* 59, No. 4, 377–399.

Gens, A. (2010), "Soil–environment interactions in geotechnical engineering," *Géotechnique* 60, No 1, pp. 3-74.

Groot, S. R. D., and Mazur, P. (1962), "Non-equilibrium thermodynamics," Amsterdam, North-Holland Pub. Co.

Houlsby, G., and Puzrin, A. M., (2007), "Principles of Hyperplasticity: An Approach to Plasticity Theory Based on Thermodynamic Principles," Springer-Verlag London.

Hueckel, T. & Borsetto, M. (1990) "Thermoplasticity of saturated soils and shales: Constitutive equations," *ASCE Journal of Geotechnical Engineering*, 116(2), 1765-1777.

Hueckel, T. & Baldi, G. (1990), "Thermoplasticity of saturated clays: experimental constitutive study," *J. Geotech. Engng ASCE* 116, No. 12, 1768–1796.

Hueckel, T., Pellegrini, R. and Del Olmo, C. (1998), "A constitutive study of thermo-elastoplasticity of deep carbonatic clays," *International Journal for Numerical and Analytical Methods in Geomechanics*, 22(7), 549-574.

Hueckel, T. A. (1992), "Water-mineral interaction in hygromechanics of clays exposed to environmental loads: a mixture-theory approach," *Can. Geotech. J.*, 29, 1071-1086.

Jâky, J. (1944), "A nyugalmi nyomâs tényezöje (The coefficient of earth pressure at rest)," *Magyar Mérnok és Epitész Egylet Közlönye (Journal for Society of Hungarian Architects and Engineers)*, October, pp. 355-358.

Jiang, Y., and Liu, M. (2007), "From elasticity to hypoplasticity: dynamics of granular solids," *Phys Rev Lett*. 99(10): 105501

Jiang, Y., and Liu, M. (2009), "Granular solid hydrodynamics," *Granular Matter*, 11(3), 139–156, 2009.

Ladd, C. C., and DeGroot, D. J. (2003), "Recommended Practice for Soft Ground Site Characterization: Arthur Casagrande Lecture," In *12th Panamerican Conference on Soil Mechanics and Geotechnical Engineering*, Vol. 1, pp. 1-57.

Laloui, L. and Francois, B. (2009), "ACMEG-T: Soil thermoplasticity model," *Journal of Engineering Mechanics-ASCE*, 135(9), 932-944.

Laloui, L., Moreni, M. and Vulliet, L. (2003), "Behavior of a dual-purpose pile as foundation and heat exchanger," *Canadian Geotechnical Journal*, 40(2), 388-402, doi: 10.1139/T02-117.

Laloui, L., Nuth, M. and Vulliet, L. (2006), "Experimental and numerical investigations of the behaviour of a heat exchanger pile," *International Journal for Numerical and Analytical Methods in Geomechanics*, 30(8), 763-781, doi: 10.1002/Nag.499.

Lambe, T.W. (1960), "The structure of compacted clay," *ASCE Journal of the Soil Mechanics and Foundation Engineering Division*, 125: 682–706.

Leroueil, S. & Marques, M. E. S. (1996)," Importance of strain rate and temperature effects in Geotechnical Engineering," *ASCE Measuring and Modeling Soil Behavior (GSP 61),* 1-60.

Mackenzie, R. C. (1958), "Density of water sorbed on montmorillonite," *Nature,* v. 181, p. 334.

Mitchell, J. K. (1993), "Fundamentals of soil behavior, 2nd edn.," Wiley New York.

Mooney, R. W., Keenan, A. G., and Wood, L. A. (1952), "Adsorption of water vapor on montmorillonite," *Journal of the Americal Chemical Soc*iety, Vol. 74, pp. 1371-1374.

Morin, R., and Silva, A. J. (1984), "The effects of high pressure and high temperature on some physical properties of ocean sediments," *Journal of Geophysical Research*, 89(B1), pp. 511–526.

Norrish, K. (1954), "The swelling of montmorillonite," *Faraday Society Discussion,* no. 18, pp. 120-134.

Paaswell, R.E. (1967), "Temperature effects on clay soil consolidation," *Journal of the Soil Mechanics and Foundation Engineering Division, ASCE,* 93(SM3): 9–22.

Panagiotidou, A. I. (2017), "Adaptation of Granular Solid Hydrodynamics for Modeling Sand Behavior", *Ph.D. Thesis,* Massachusetts Institute of Technology.

Smith, D. W., and Booker, J. R. (1989), "Boundary integral analysis of transient thermoelasticity," *International Journal for Numerical and Analytical Methods in Geomechanics, 13*(3), 283-302.

Sposito, G. (1984), "The surface chemistry of soils," Oxford University Press.

Sposito, G. & Prost, R. (1982), "Structure of water adsorbed on smectites," *Chem. Rev*. 82, No. 6, 553–573.

Suter, J. L., Coveney, P. V., Greenwell, H. C., and Thyveetil, M. A. (2007), "Large-Scale Molecular Dynamics Study of Montmorillonite Clay: Emergence of Undulatory Fluctuations and Determination of Material Properties," *J. Phys. Chem. C,* 111, 8248-8259.

Zhang Z. & Cheng X. (2013), "Simulation of nonisothermal consolidation of saturated soils based on a thermodynamic model," *Scientific World Journal*, Hindawi Publishing Co., http://dx.doi.org/10.1155/2013/192163.

Zhang Z. & Cheng X. (2017), "A Fully Coupled THM Model Based on a Non-equilibrium Thermodynamic Approach and its Application," *Int. J. Numer. Anal. Meth. Geomech.*, Vol. 41(4), pp. 527 – 554.

Zymnis, D. M. & Whittle, A. J. (2014), "Numerical Simulation of a Shallow Geothermal Heating/Cooling System," *Proc. ASCE GeoCongress GSP 234*, 2767-2776.

Zymnis, D. M. (2016), "Long-Term Ground Response For Borehole Heat Exchangers In Clay", *Ph.D. Thesis*, Massachusetts Institute of Technology.

Zymnis, D. M., Whittle, A. J. and Germaine, J. T., (2019a), "Measurements of Temperature-Dependent Bound Water in Clays," *ASTM Geotechnical Testing Journal*, Vol. 42(1), https://doi.org/10.1520/GTJ20170012.

Notation

Lower Case

a	TTS model input constant that controls rate effects
c	TTS model input constant related to cohesion
c’	TTS model input constant related to the critical state friction angle
e	Void ratio
h	TTS model input constant that controls hysteretic strains
m_1	TTS model input constant that controls elastic strain evolution
m_2	TTS model input constant that controls elastic strain evolution and location of reload curve
m_3	TTS model input constant that controls the contribution of volumetric and deviatoric strains on granular temperature production
m_4	TTS model input constant that controls the rate of granular temperature production
m_5	TTS model input constant that controls the amount of thermal volumetric strains produced due to heating and cooling
p	Mean total stress
p’	Mean effective stress
q	Shear stress
w	Water content

Upper Case

B_0	TTS model input constant that controls location of VCL
B_1	TTS model input constant that controls slope of VCL
C_c	Compressibility index
G_s	Specific gravity of soil
$\dot{I}_g$	Granular entropy conversion rate
K_0	In-situ coefficient of earth pressure at rest
K_e	Secant elastic bulk modulus of the solid skeleton
L_T	TTS model input constant that controls the shift of the VCL due to increase in temperature
M	Slope of Critical State Line
T	Temperature
T_{cyc}	Imposed range of temperature during cyclic heating and cooling

T_g	Granular Temperature

Greek

α_{bf}	Input constant for TTS model that controls the conversion of bound to free water during heating
β	Thermal expansion coefficient
ε_s	Deviatoric strain
ε_v	Volumetric strain
ξ	TTS model input constant that controls the coefficient of earth pressure at rest K_0
ρ	Mass density
ρ_d	Dry density of soil medium
σ'_h	Horizontal effective stress
σ'_{oct}	Mean effective stress
σ'_p	Preconsolidation pressure
σ'_v	Vertical effective stress
φ	Porosity
ω_e	Elastic Potential Energy Density Function

Superscripts

D	Irreversible
e	Elastic
h	Hysteretic

Subscripts

0	Reference initial state
20	At temperature 20°C
bw	Bound water
fw	Free water
NC	Normally consolidated
OC	Overconsolidated
s	Soil skeleton or solid particles
w	Water

Abbreviations

CSL	Critical State Line
NC	Normally consolidated

OC	Overconsolidated
OCR	Overconsolidation Ratio
SSA	Specific Surface Area
SQD	Specimen Quality Designation
TTS	Tsinghua ThermoSoil Model
VCL	Virgin Consolidation Line

Table 1: State variables used in TTS model

Loading		
$\dot{\varepsilon}_v, \dot{\varepsilon}_s$	1/s	Volumetric and deviatoric total strain rate
$\dot{T}_v$	°C/s	Temperature rate
State Variables		
ϕ_{bw}, ϕ_{fw}	-	Bound and free water porosity
$\varepsilon_v^e, \varepsilon_s^e$	-	Volumetric and deviatoric elastic strains
$\varepsilon_v^h, \varepsilon_s^h$	-	Volumetric and deviatoric hysteretic strains
T_g^*	$1/s_2$	Granular temperature
Deduced Variables		
ρ_d	kg/m^3	Dry density

e	-vVoid ratio	

* Dimensions correspond to rate independence (a = 0.5)

Mechanical Properties			
Calibrated Parameters[+]			
B_0	Pa	Location of VCL	3.8×10^{-4}
B_1	m^3/kg	Slope of VCL	0.0162
h	-	Hysteretic strains (slope of unload curve)	0.05
m_2	- *	Controls elastic strain evolution and location of reload curve	150
c'	-	Affects critical state response	0.0758
ξ	-	Sets coefficient of earth pressure at rest K_0	0.1
Predetermined parameters for clay			
m_3	-	Controls contribution of volumetric and deviatoric strains on granular temperature production	1.0
m_4	$kg\ s^{-1}m^{-3}$ *	Rate of granular temperature production	6.0×10^{4}
a	-	Controls rate effects (a = 0.5 for rate independence)	0.5
c	-	Cohesion (c=0 for sands)	0.01
$m_{1,0}$	-	Controls elastic strain evolution	1.0
Thermal Properties[++]			
α_{bf}	$°C^{-1}$ +++	Affects conversion of bound water to free water during heating	0.0237
m_5	$s^3\ m^{-2}\ °C^{-1}$ *	Controls amount of thermal volumetric strains produced due to heating and cooling cycles	0.1
L_T	$°C^{-1}$	Controls temperature dependence of VCL	0.02
$\beta_{s,vol}$	$°C^{-1}$	Volumetric thermal Expansion of solid particles	1.8×10^{-5}

* Dimensions corresponding to rate independence (a = 0.5)
+ From sample S4b (Figures 8 - 11)
++ From sample S3 (Figures 13 and 14)
+++ From lab measurements (Zymnis et al., 2019a)

Table 2: Input constants used in TTS model and calibrated parameters for Geneva clay

	S3	S4b
Depth, z [m]	14.3 – 14.6	15.1 – 15.4
In-situ pore water pressure, p_w [kPa][1]	144.9	152.5
In-situ total vertical stress, σ_v [kPa]	294.1	305.0
In-situ effective vertical stress, σ'_v [kPa]	149.2	152.2

OCR [-]	1.0	1.0
Water content, w [%]	23.2 – 26.3	27.9
Soil Mass Density, ρ [kg/m^3]	1980 – 2080	1930
Solid particle mass density, ρ_s [kg/m^3]	2780	2710
Dry density, ρ_d [kg/m^3]	1590 – 1690	1510
Degree of saturation, S_r [%]	94.6 – 100	94.9
Liquid limit, w_L [%]	34.0	42.6
Plasticity Index, I_p [%]	12.8	18.4
[1] Water table at the surface level		

Table 3: In-situ state of stress and identification properties of the tested soil samples (after Di Donna and Laloui, 2015)

Test Number	Material	Type*	Temperature, T [°C]	Vertical eff. stress, σ'_v [kPa]	OCR before thermal cycles
1	S3	SO	20	1 – 1000 – 60	-
2	S3	TO	40	1 – 1000 – 60	-
3	S3	TO	60	1 – 1000 – 60	
		+(TC)	(5 – 60)		(16.0)
7	S3	TC	5 - 60	125	1.0
10	S4b	TC	5 - 60	125	1.0
		+(SO)		(1000 – 60)	(-)
* SO = Standard Oedometer, TO = Thermal Oedometer, TC = Thermal Cycles					

Table 4: Experimental program undertaken by Di Donna and Laloui (2015)

Figure 1: Solid, free water and bound water phases assumed in TTS model (after Cekerevac, 2003)

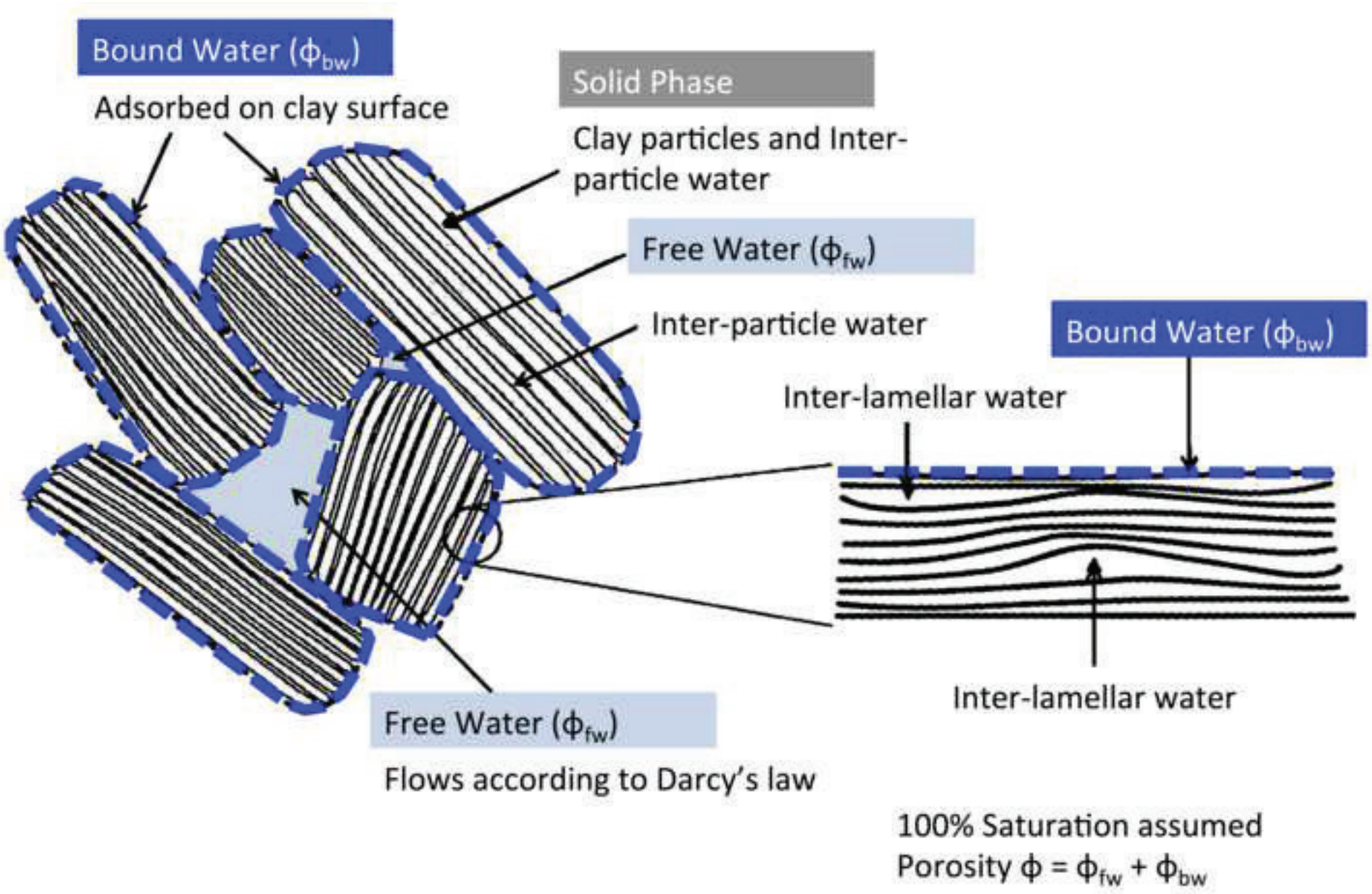

Figure 2: Effect of temperature on bound water content as predicted from lab measurements (after Zymnis et al., 2019a)

Click here to access/download;Figure;Figure02.tiff

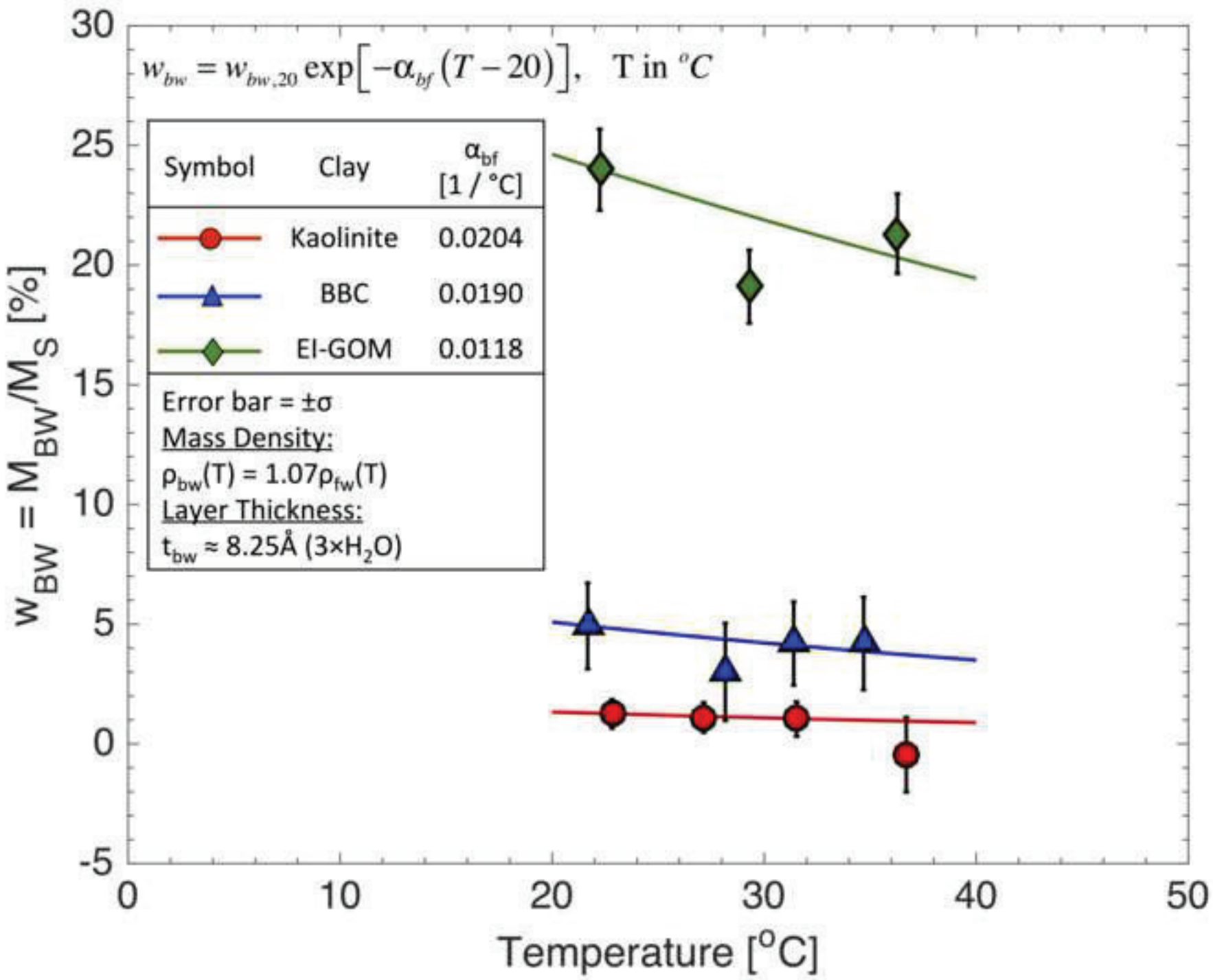

Figure 3: Double entropy concept assumed in TTS model (after Zhang and Cheng, 2012)

Click here to access/download;Figure;Figure03.tiff

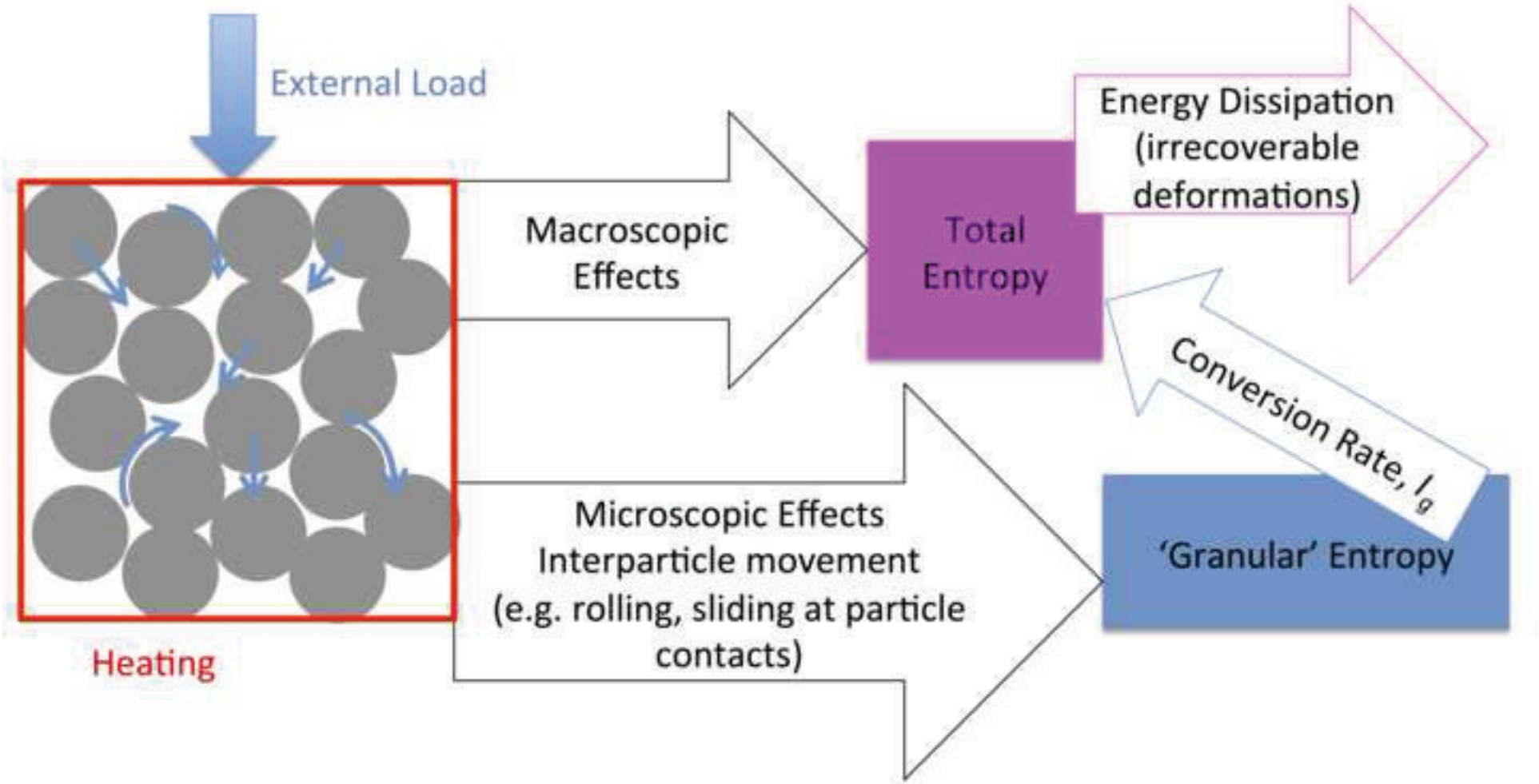

Figure 4: Effect of hysteretic strain on strain accumulation due to cyclic loading and unloading (after Zhang and Cheng, 2017)

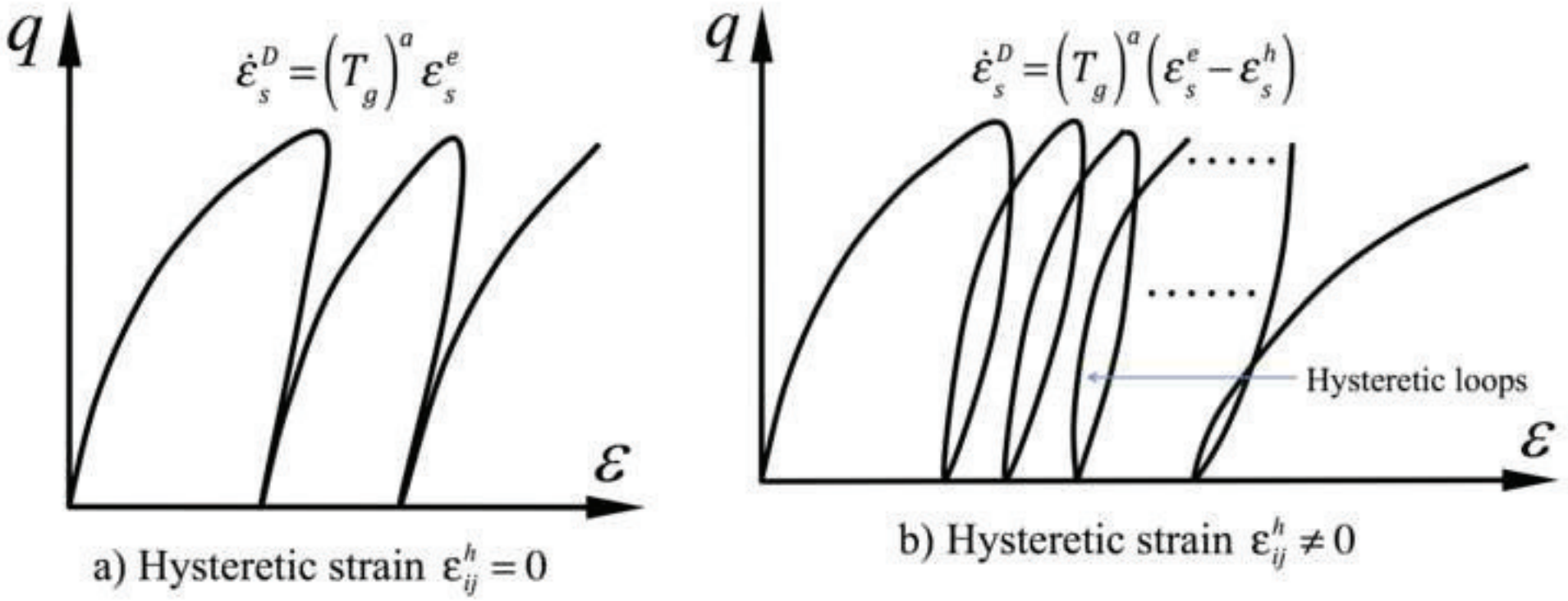

Figure 5: Effect of parameter m4 on transient response of TTS model

Click here to access/download;Figure;Figure05.tiff

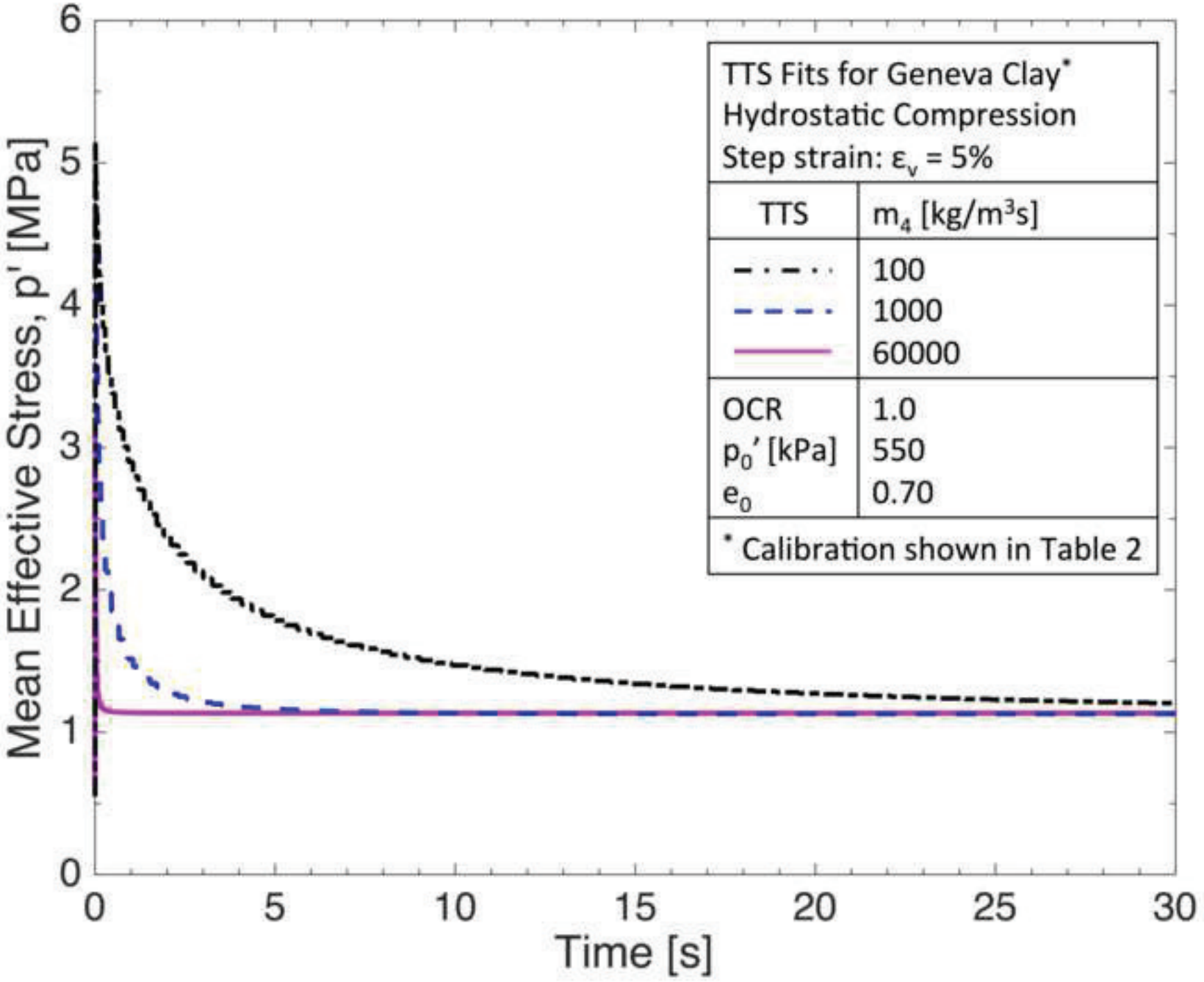

Figure 6: Experimental measurements on Geneva Clay (after Di Donna and Laloui, 2015)

Click here to access/download;Figure;Figure06.tiff

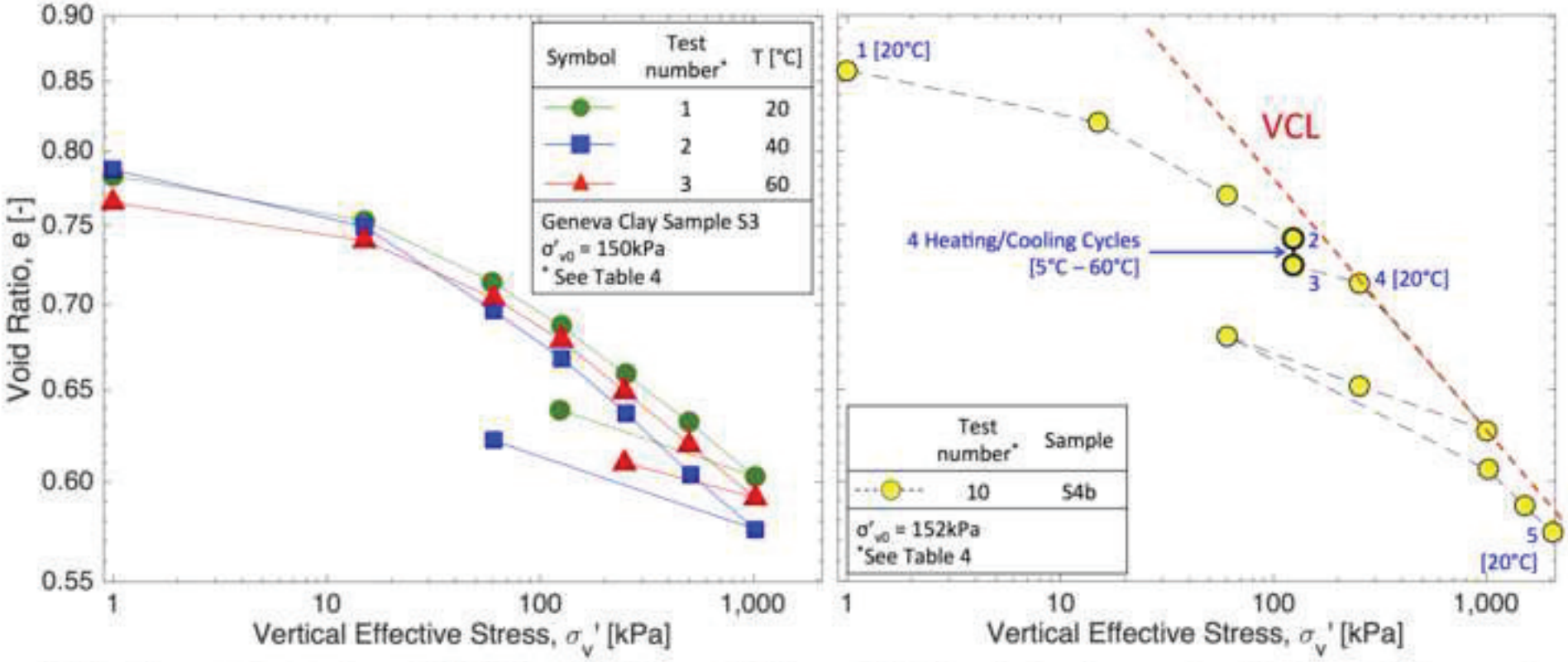

a) Oedometric tests at 20 °C, 40 °C and 60 °C on S3 samples

b) Combined mechanical and thermal cyclic loading on S4b sample

Figure 7: Geneva clay response to thermal cycles (after Di Donna and Laloui, 2015)

Click here to access/download;Figure;Figure07.tiff

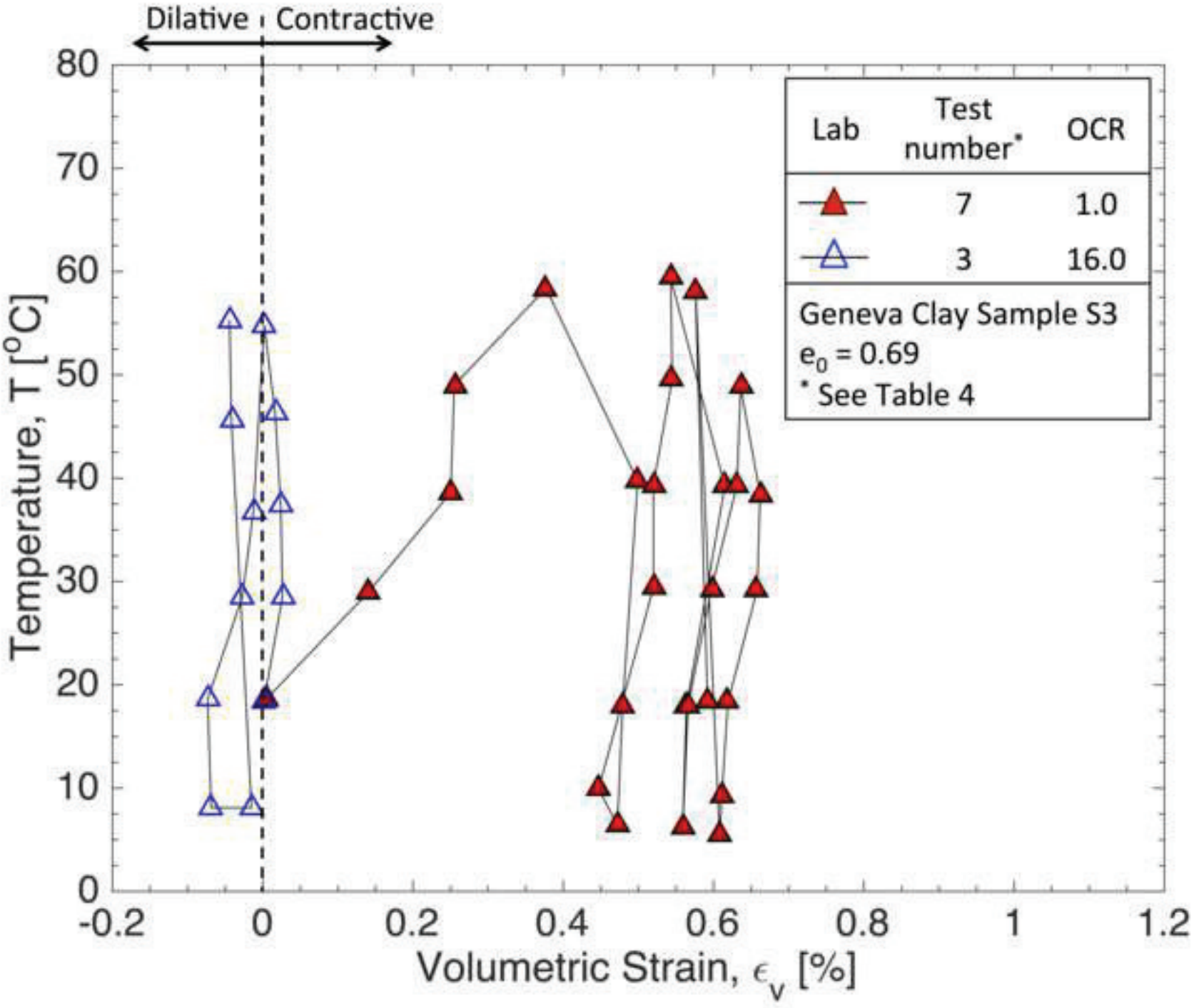

Figure 8: Effect of B1 on slope of normalized virgin consolidation line (VCL)

Click here to access/download;Figure;Figure08.tiff

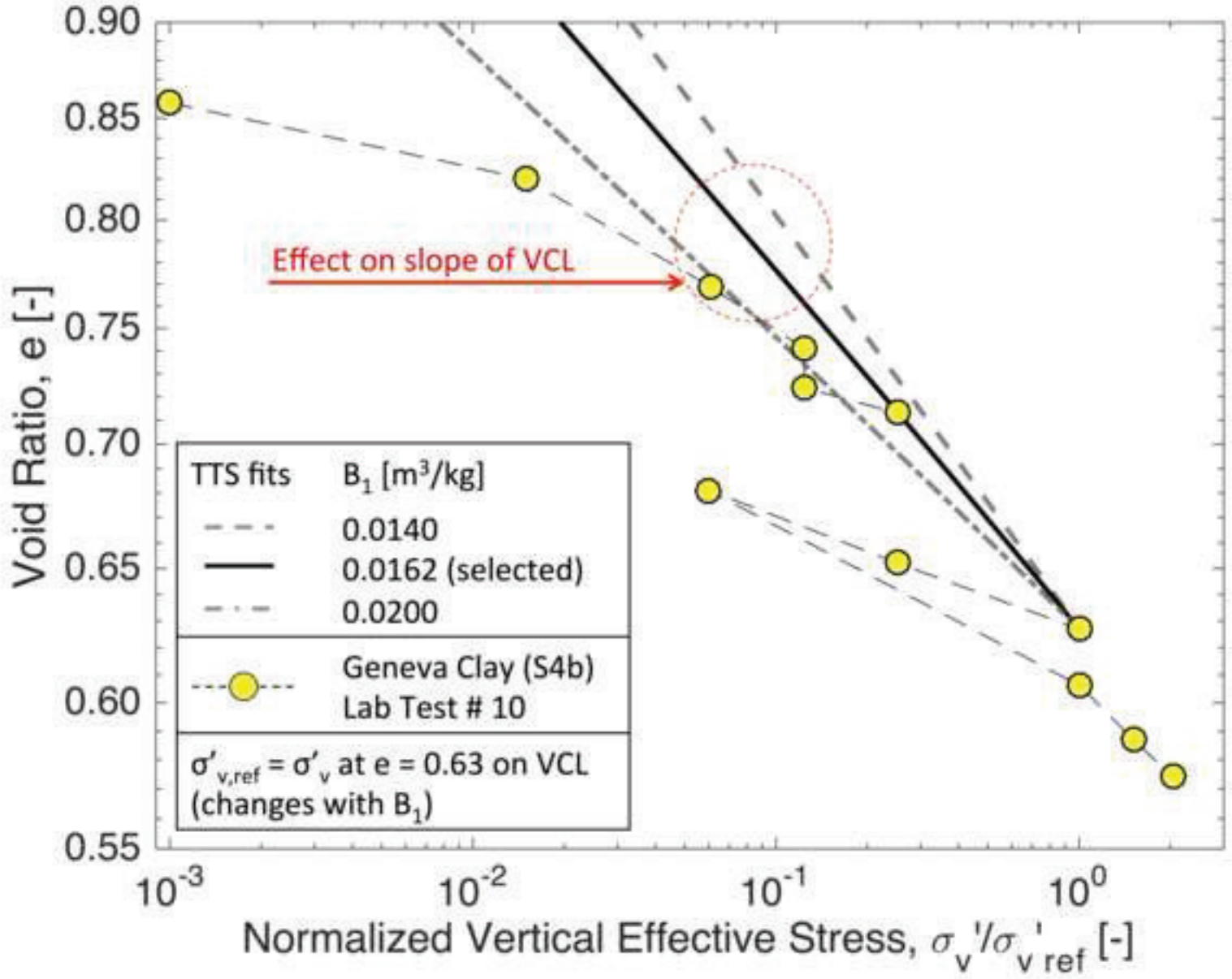

Figure 9: Calibration of TTS model parameters h and m2 for Geneva clay

Click here to access/download;Figure;Figure09.tiff

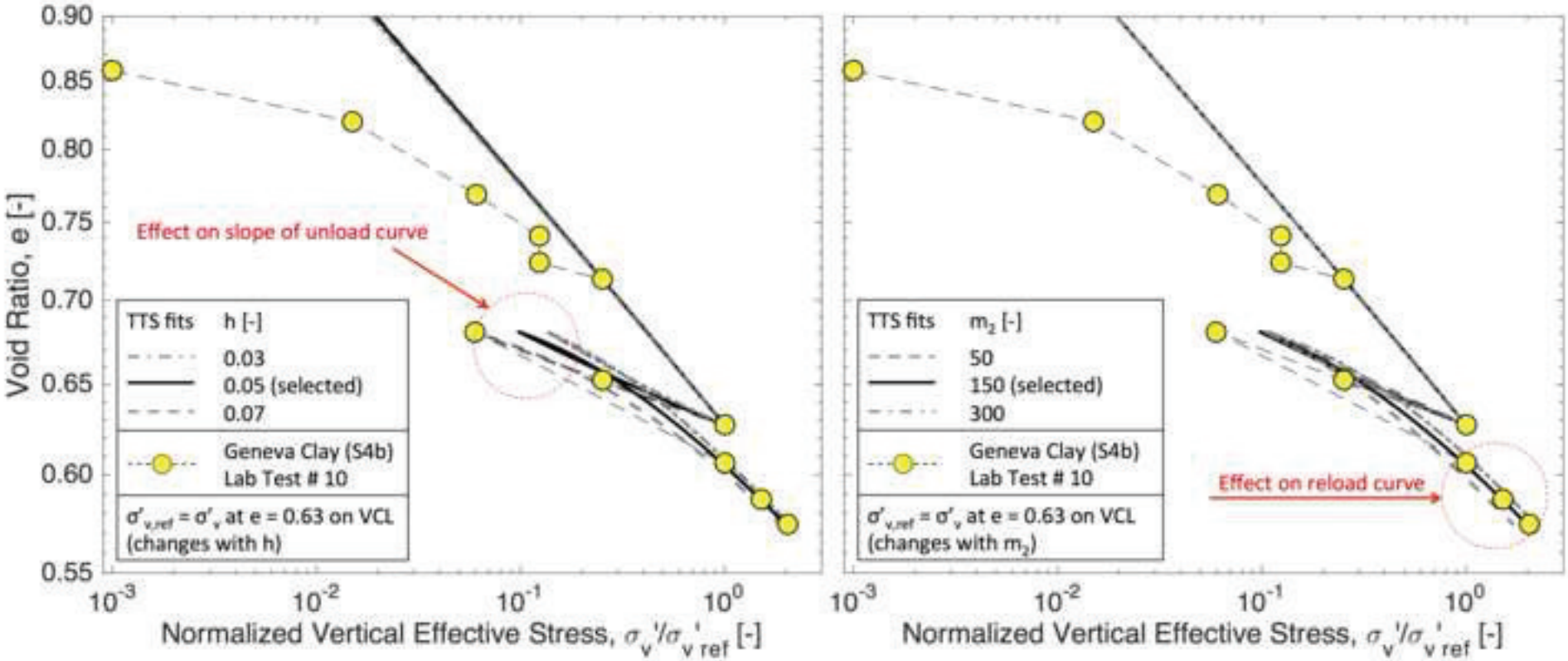

a) Effect of h on unload curve

b) Effect of m_2 on reload curve

Figure 10: Effect of ξ on computed coefficient of earth pressure at rest K0NC

Click here to access/download;Figure;Figure10.tiff

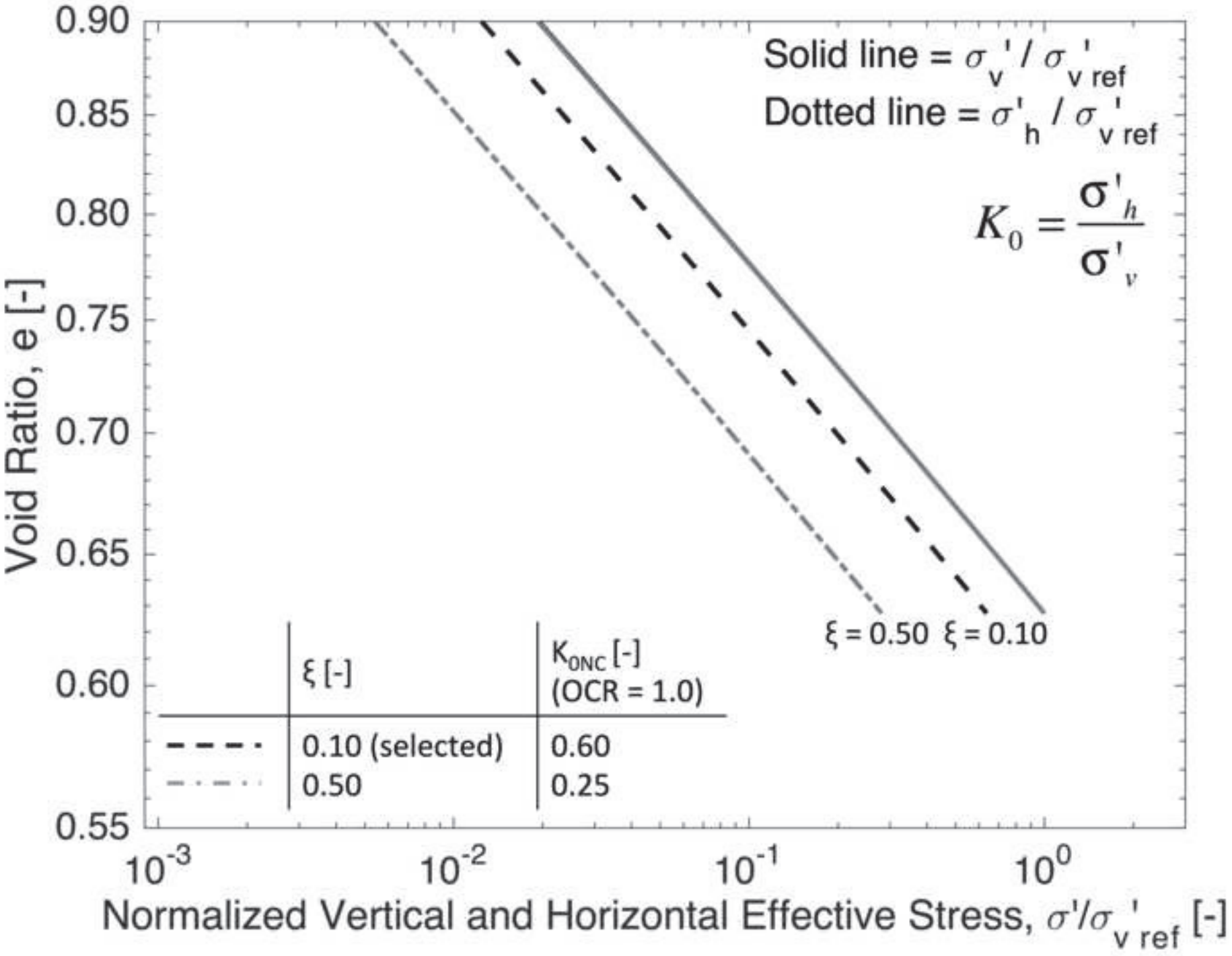

Figure 11: Effect of B0 on the location of the VCL

Click here to access/download;Figure;Figure11.tiff

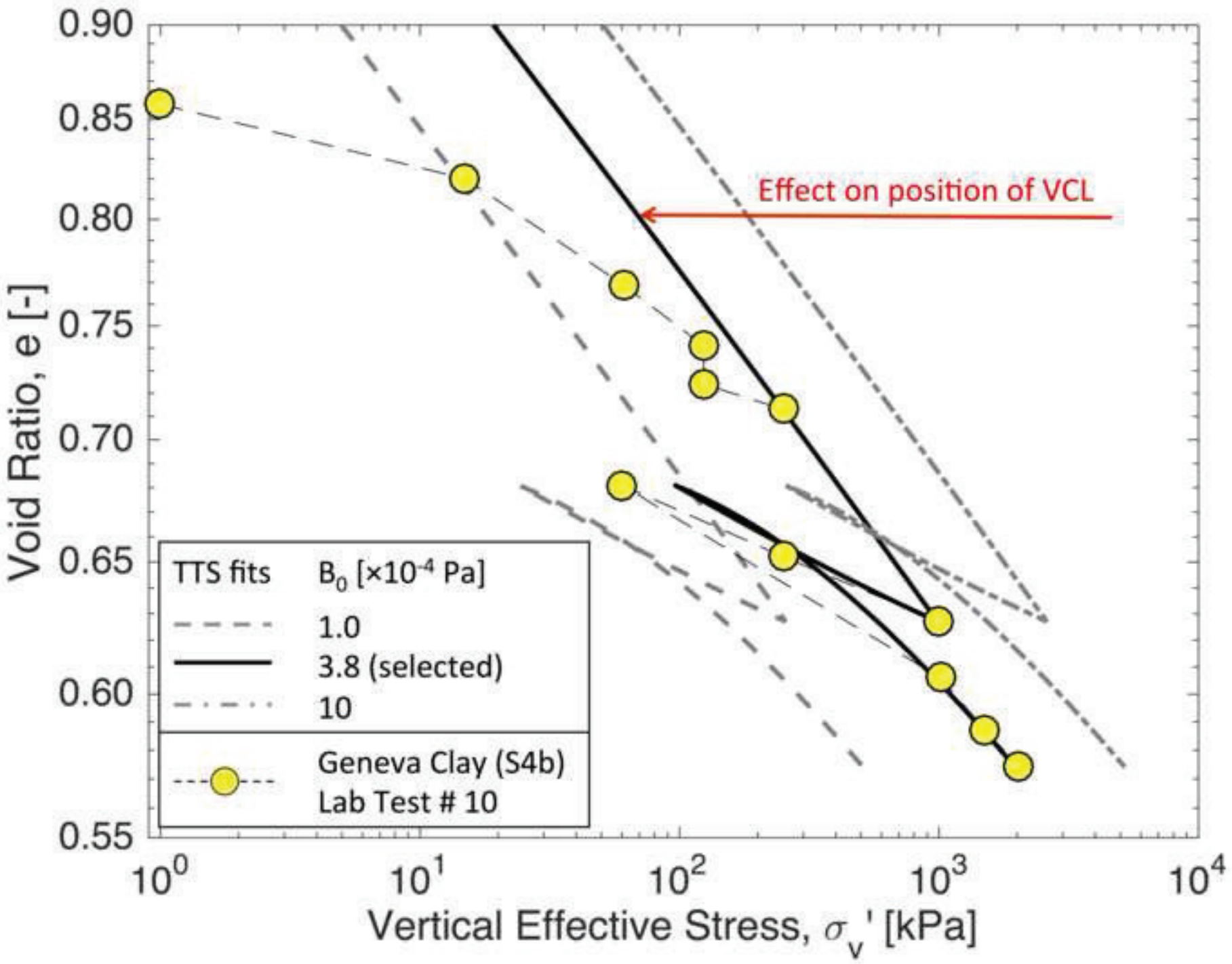

Figure 12: Resulting TTS fit to Geneva Clay sample S4b and evolution of strain state variables using calibrated parameters shown in Table 2

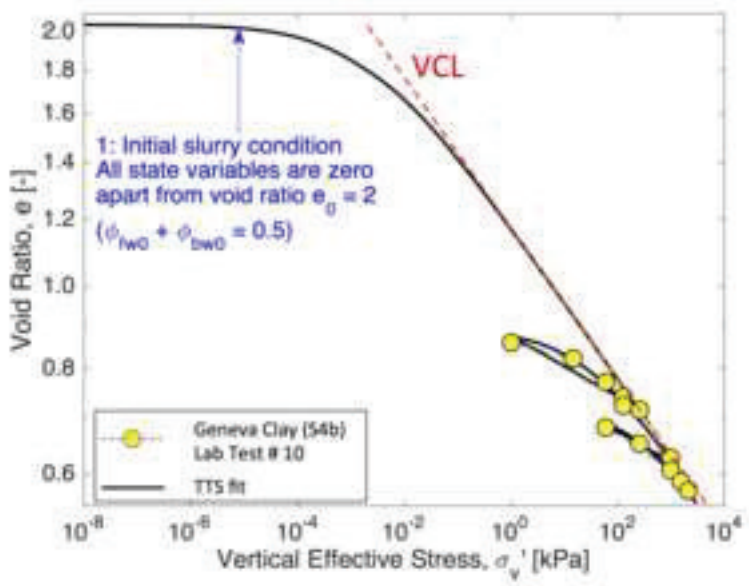

a) Slurry condition at start of calibration

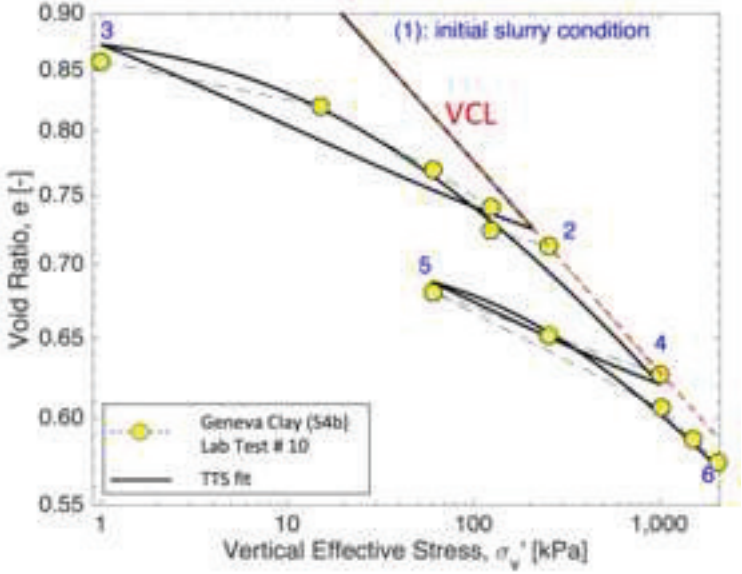

b) Zoomed-in figure showing sequence of loading-unloading-reloading steps

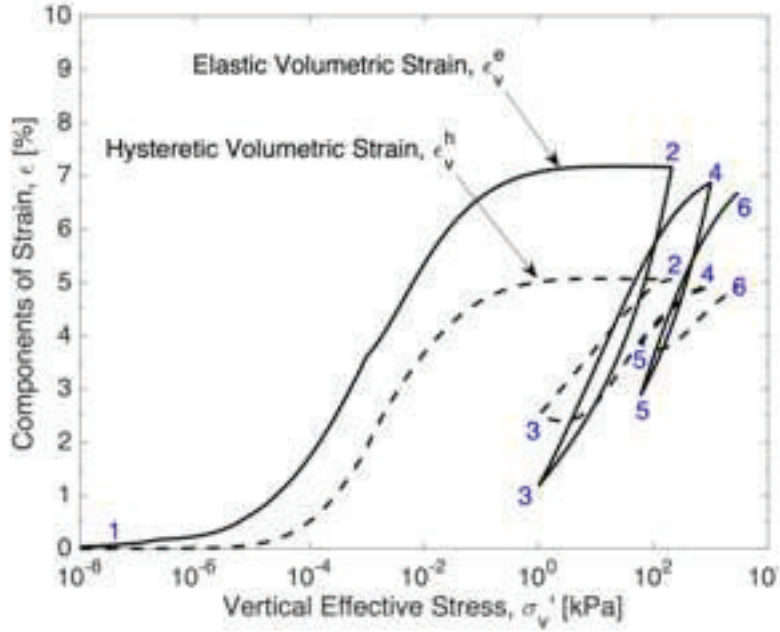

c) Volumetric Strain, ε_v

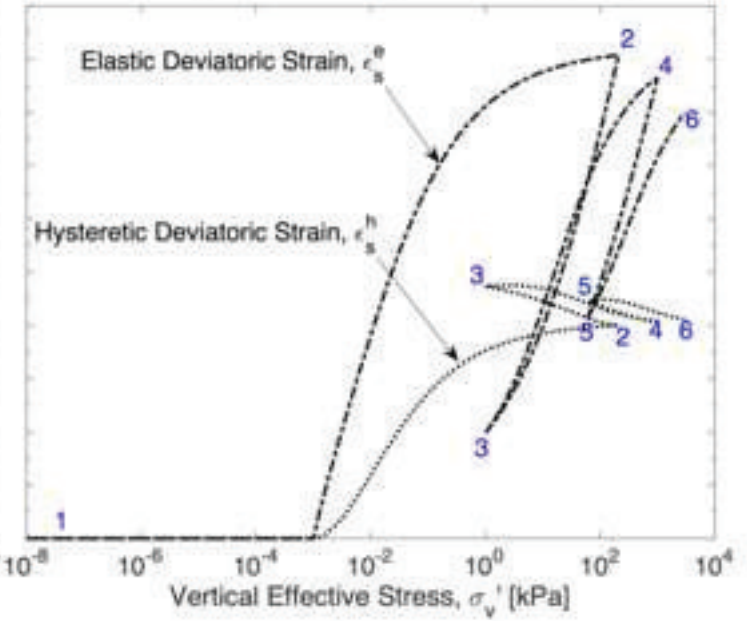

d) Deviatoric Strain, ε_s

Figure 13: Effect of parameter LT on temperature dependence of the VCL and comparison to Geneva Clay lab measurements

Click here to access/download;Figure;Figure13.tiff

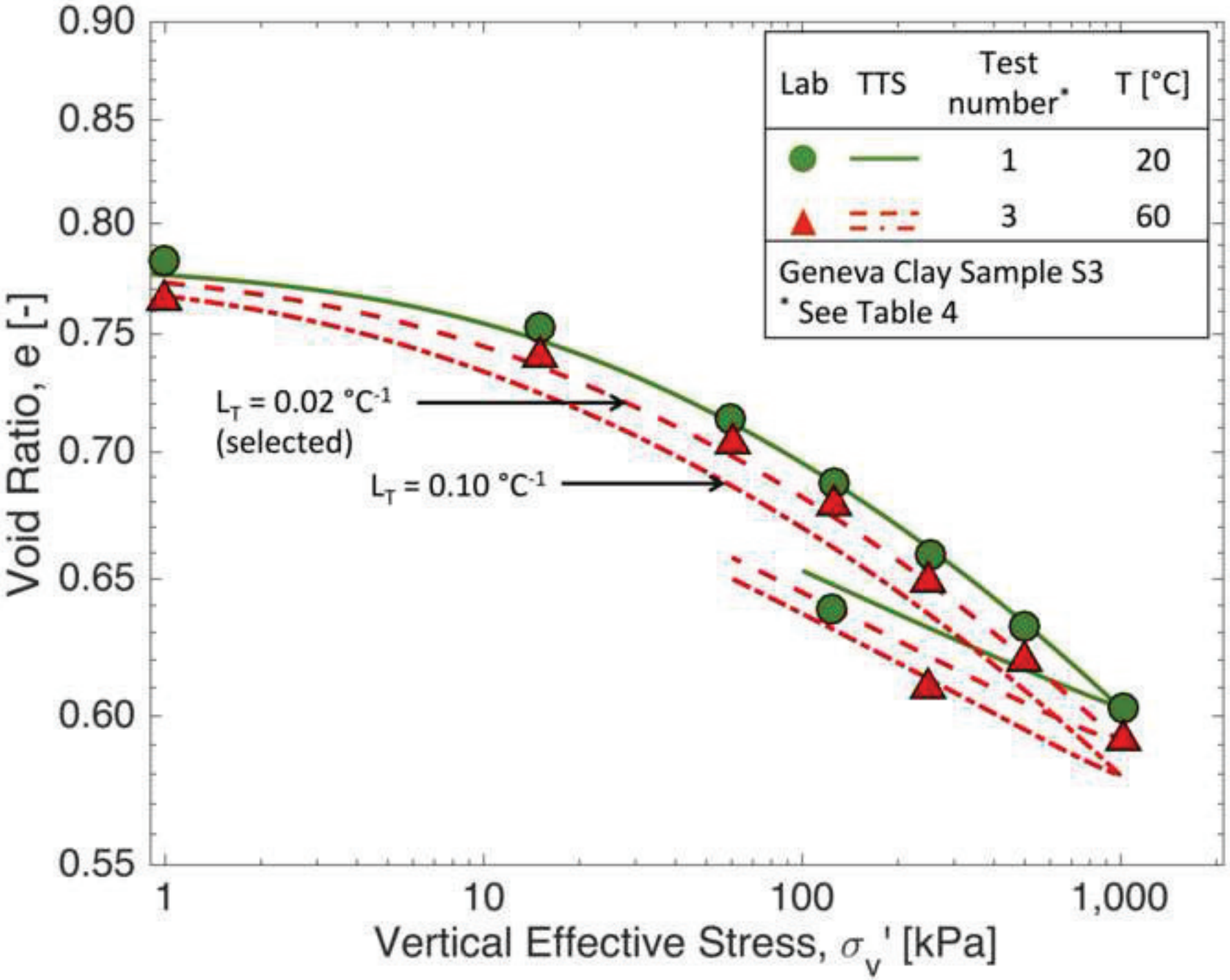

Figure 14: Effect of m5 on simulated accumulation of thermal volumetric and comparison to Geneva Clay lab measurements

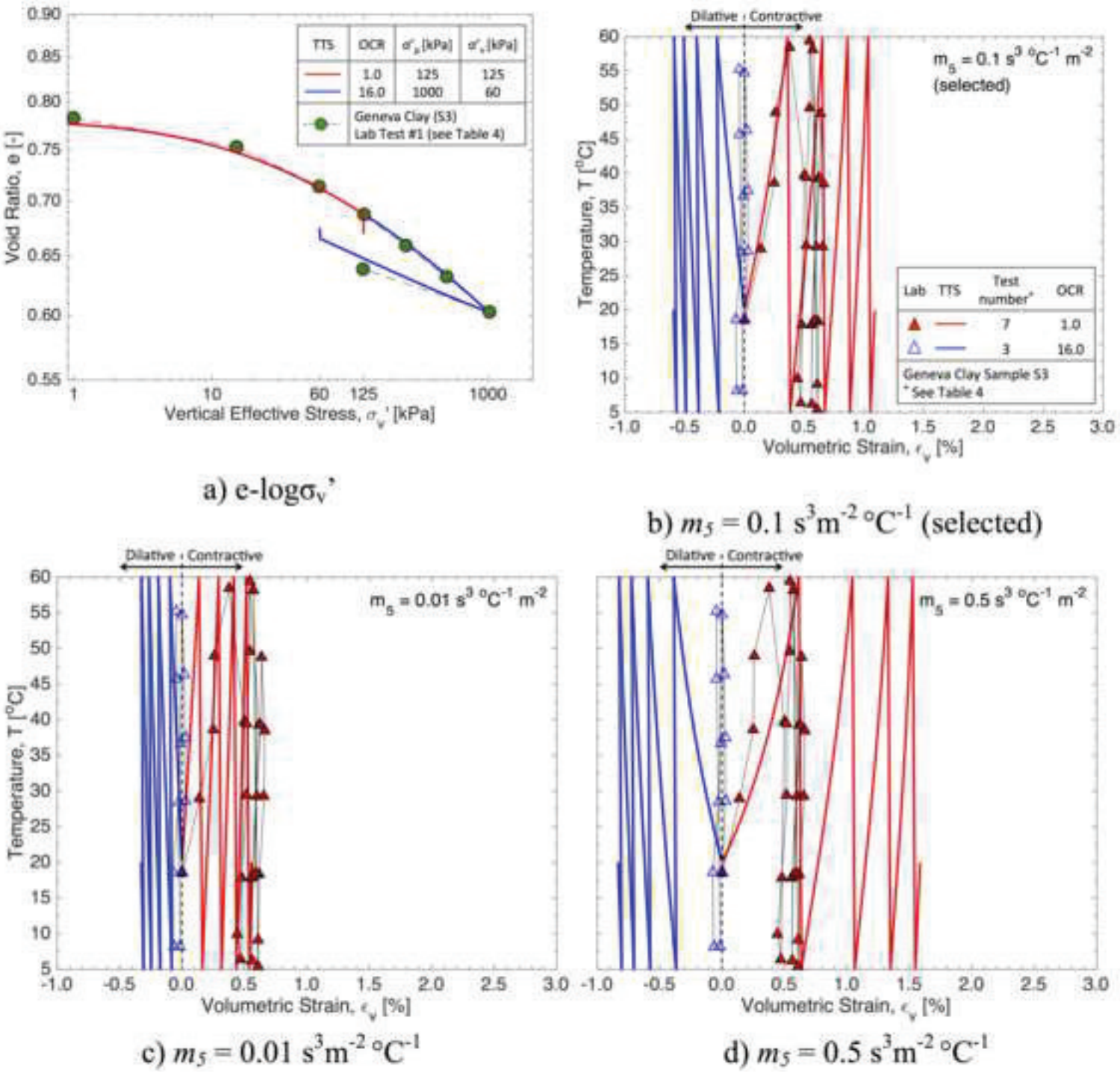

Figure 15: TTS model simulation of thermal volumetric strains produced due to one heating-cooling cycle for Geneva clay of

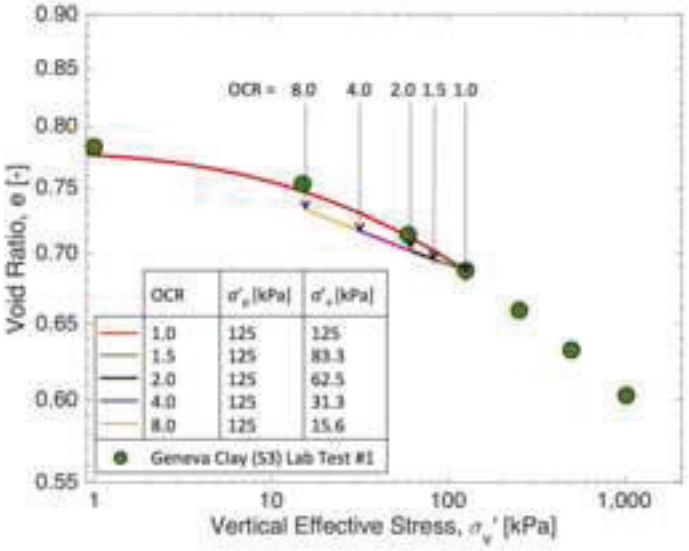

a) e-logσ_v'

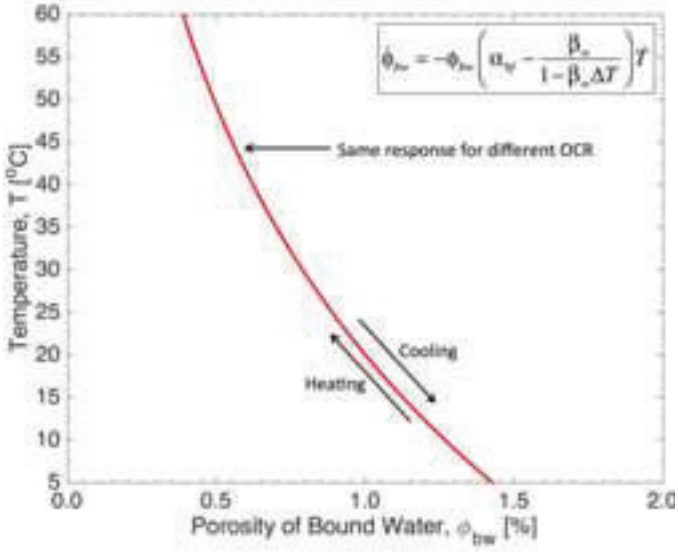

b) Bound Water Porosity, φ_{bw} vs temperature

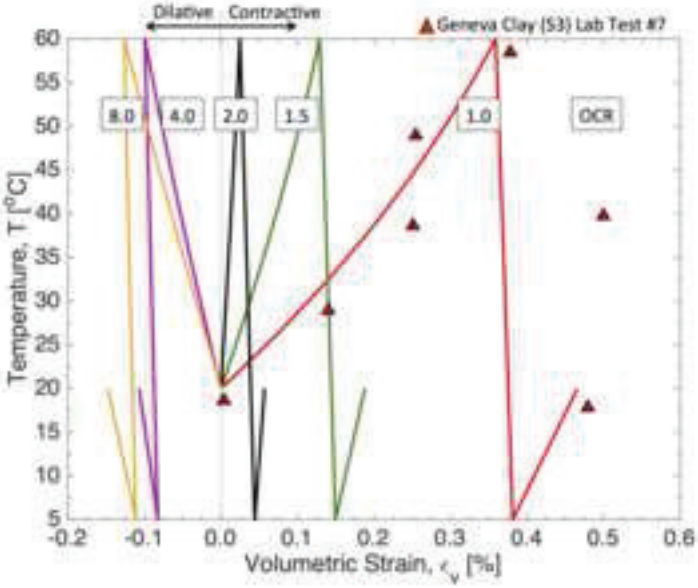

c) Temperature vs thermal ε_{vol}

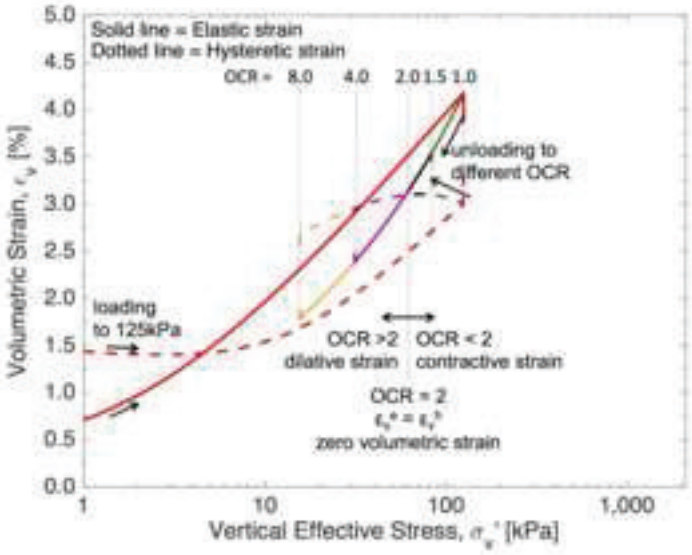

d) Illustration of TTS response based on volumetric strains

Figure 16: TTS model simulation of accumulated thermal volumetric strains produced due to long-term cyclic heating and cooling of Geneva clay of different OCR

Click here to access/download;Figure;Figure16.tiff

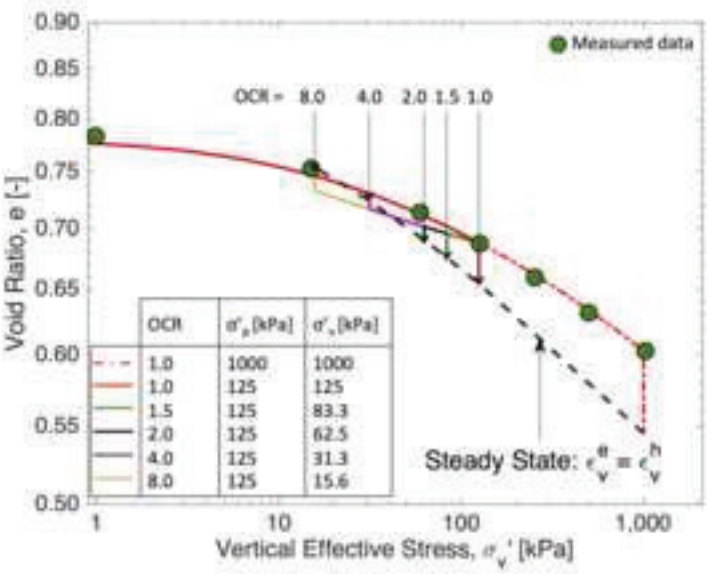

a) e-logσv'

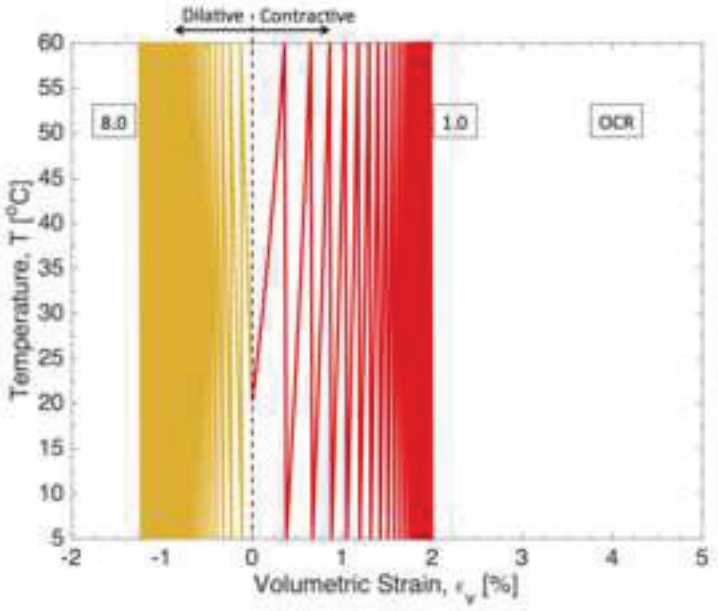

b) Temperature vs thermal ε_{vol}

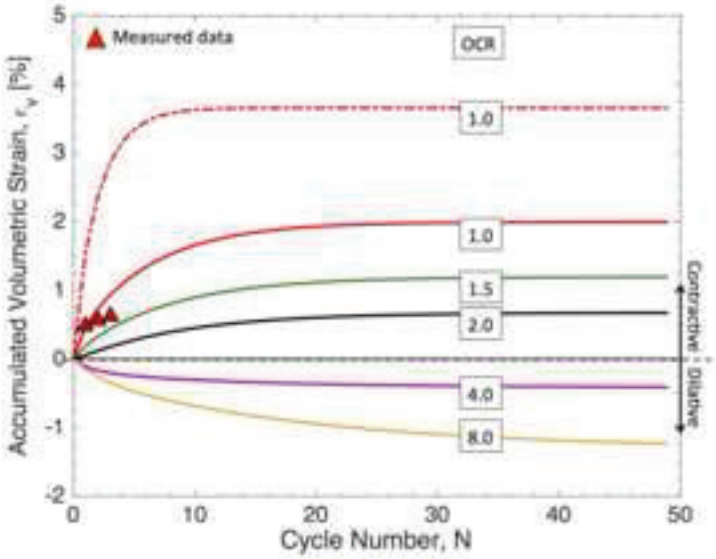

c) Accumulation versus cycle number

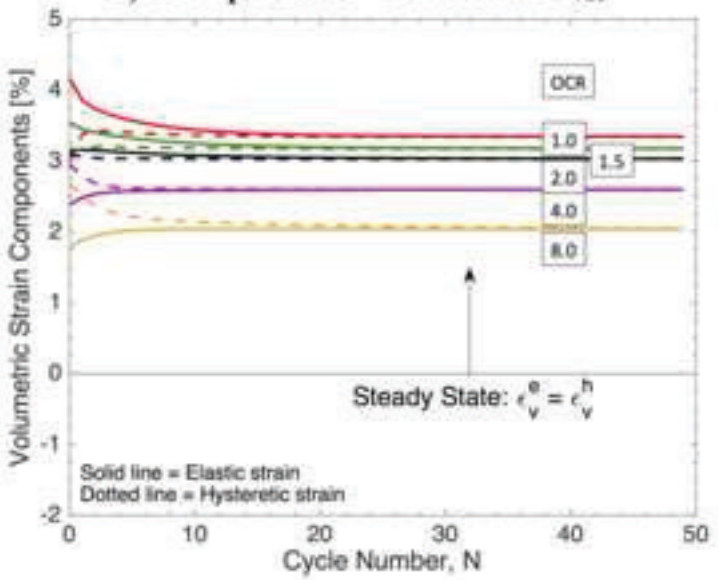

d) Explanation of TTS response based on volumetric strains

Figure 17: TTS model simulation of thermal volumetric strains produced due to long-term cyclic heating and cooling of NC Geneva clay with different Tcyc

Click here to access/download;Figure;Figure17.tiff

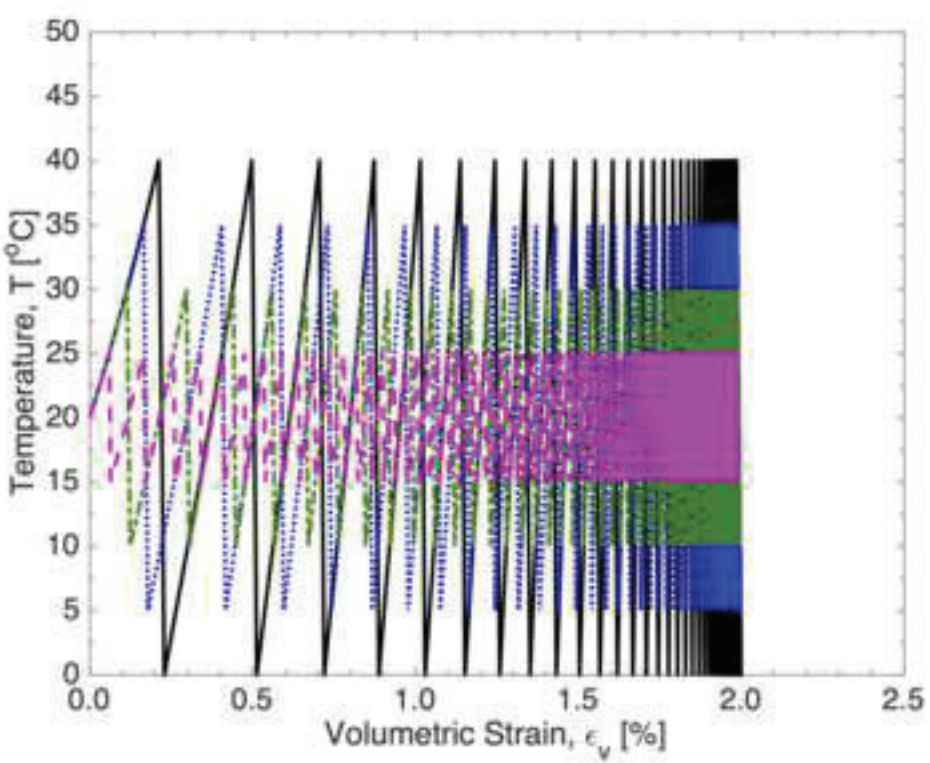

a) T vs ε_v

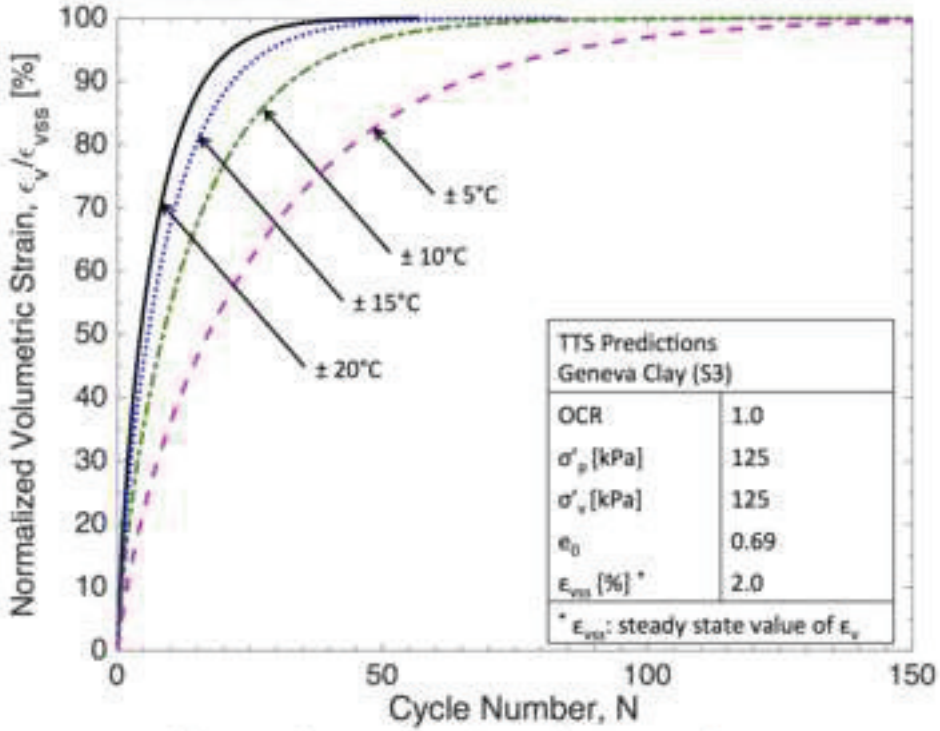

b) $\varepsilon_v / \varepsilon_{vss}$ vs Cycle Number